Materials Advances

ROYAL SOCIETY OF CHEMISTRY

REVIEW

View Article Online
View Journal

Cite this: DOI: 10.1039/d6ma00011h

Current advances, limitations, and future perspectives of MOF-based versatile delivery platforms for cancer therapy

Luan Minh Nguyen, †[a] Giao Thuy Quynh Vu, †[a] Ngoan Thi Thao Nguyen,[b] Thuy Thi Thanh Nguyen,[b] Duyen Thi Cam Nguyen,[c] Thuan Van Tran,[c] Ngoc Hoi Nguyen[a] and Dai Hai Nguyen *[a]

Received 4th January 2026,
Accepted 23rd March 2026

DOI: 10.1039/d6ma00011h

rsc.li/materials-advances

Metal–organic frameworks (MOFs) are emerging as highly versatile nanoplatforms for cancer therapy. Their large surface area, adjustable porosity, and tunable chemistry allow efficient loading of many therapeutic cargos. MOFs also interact closely with key features of the tumor microenvironment, such as pH, hypoxia, redox conditions, adenosine triphosphate concentration, and ionic imbalance. These interactions enable controlled and stimulus-responsive release. Recent studies have demonstrated the ability of MOF-based systems to deliver drugs, nucleic acids, proteins, and therapeutic gases with improved therapeutic performance. Multi-cargo strategies further enhance anticancer efficacy by combining complementary mechanisms in a single platform. This review summarizes these advances and highlights the potential of MOFs to support precise and effective cancer treatment. Continued progress in this field may accelerate the development of next-generation MOF-based therapeutic systems for clinical applications.

1. Introduction

Cancer remains one of the leading causes of mortality worldwide, and the complexity of its pathophysiology continues to challenge the development of effective therapeutic strategies.[1,2] Conventional drug delivery systems are often subjected to rapid clearance and limited physicochemical stability.[3] Non-specific biodistribution and inadequate accumulation in tumor tissues further reduce therapeutic outcomes and increase the likelihood of dose-related toxicity.[4] These challenges highlight the urgent need for advanced delivery platforms capable of precise targeting, controlled release, and transport of diverse therapeutic agents such as drugs, nucleic acids, proteins, and gasotransmitters.

Metal–organic frameworks (MOFs) have emerged as a promising class of crystalline porous materials. MOFs consist of metal ions or clusters coordinated with organic linkers, forming highly ordered networks with tunable pore structures, large surface areas, and extensive chemical versatility.[5–7] The modular architecture of MOFs supports the encapsulation of a broad range of therapeutic cargoes.[8] Responsiveness to pathological cues in the tumor microenvironment, such as acidic pH, redox gradients, hypoxia, and enzymatic activity, provides additional advantages for controlled and site-specific release.[9,10] Structural tunability and multifunctionality distinguish MOFs from conventional nanocarriers, and the integration of diagnostic and therapeutic capabilities within a single platform further expands their biomedical relevance.[11,12]

Recent advances have extended the application of MOFs beyond small-molecule drug delivery. Considerable interest has been directed toward nucleic acid transport, protein stabilization and delivery, gas therapy, and multi-cargo co-delivery for synergistic treatment outcomes.[13,14] Despite this progress, many existing reviews remain focused on traditional drug loading or single-modality therapies. Limited attention has been given to the rapidly evolving roles of MOFs in advanced delivery technologies. Insufficient discussion also exists regarding the dynamic interactions between MOFs and tumor-associated conditions, indicating a clear need for a more comprehensive and up-to-date evaluation of next-generation MOF systems.

The present review aims to fill this gap by summarizing recent developments in MOF architectures designed for multifunctional therapeutic delivery. Key interactions between MOFs and tumor-associated conditions are described to clarify mechanisms that enable precise and stimuli-responsive release. Expanding capabilities of MOFs in transporting drugs, nucleic acids, proteins, gases, and combined therapeutic cargos are outlined to emphasize emerging therapeutic opportunities. Major limitations, translational

[a] Institute of Advanced Technology, Vietnam Academy of Science and Technology, 1B TL29 Street, An Phu Dong Ward, Ho Chi Minh City 700000, Vietnam. E-mail: nguyendaihai@iat.vast.vn, nguyendaihai0511@gmail.com
[b] Nong Lam University Ho Chi Minh City, Ho Chi Minh City 700000, Vietnam
[c] Center for Hi-Tech Development, Nguyen Tat Thanh University, Saigon Hi-Tech Park, Ho Chi Minh City 700000, Vietnam
† These authors equally contributed.

challenges, and future prospects of MOF-based delivery platforms are highlighted to support the advancement of clinically relevant MOF-enabled systems for cancer therapy.

2. Interactions between MOFs and the tumor microenvironment

The tumor microenvironment exhibits pronounced spatial and temporal heterogeneity, characterized by a wide array of features, *e.g.*, extracellular acidity, hypoxia, redox imbalance, dysregulated ATP and ion levels, elevated enzymatic and growth factor activity, receptor overexpression, and a dense extracellular matrix that restricts drug penetration.[15–17] Although these features complicate therapeutic intervention, they also provide unique biological cues for the rational design of targeted and stimulus-responsive treatment strategies. Many widely studied drug delivery platforms, such as lipid-based nanoparticles, mesoporous silica, and polymer-based nanoparticles, may require additional chemical functionalization or surface modification with specific biomolecules to achieve responsiveness to physiological stimuli within the tumor microenvironment.[18–20] Several types of MOFs, in comparison, possess intrinsically versatile architectures arising from their metal–ligand coordination chemistry. This structural tunability enables certain MOFs to respond to single or multiple tumor-associated stimuli, thereby effectively ''translating'' pathological cues into controlled therapeutic actions. Among the various features of the tumor microenvironment, five representative properties, namely pH, hypoxia, redox balance, ATP, and ions, have been particularly emphasized in the following sections.

2.1. pH

The tumor microenvironment is characterized by a distinctly lower pH compared to that of normal tissues. This phenomenon, as discussed in the Warburg effect, refers to the predominant metabolic pathway in tumor cells, where aerobic glycolysis is favored over oxidative phosphorylation. As a result, lactic acid accumulates as a byproduct of this metabolic process in the extracellular milieu, thereby reducing the pH of the tumor microenvironment to weakly acidic levels, typically ranging from 6.5 to 6.8.[21] Certain types of MOFs, on the other hand, inherently exhibit pH-responsive behavior, a property that can be exploited as a trigger for the controlled release of therapeutic payloads. This behavior originates from the coordination chemistry of MOFs constructed from organic ligands bearing proton-exchangeable functional groups. Under acidic conditions, protonation of these ligands can weaken metal–ligand coordination interactions, which may result in partial disruption of the framework structure. For example, ZIF-8, one of the most widely studied MOFs, composed of Zn^{2+} ions and 2-methylimidazole (2-MIM) ligands, was demonstrated to undergo degradation in acidic environments as a result of protonation of the imidazole groups in 2-MIM.[22] Similarly, the structure of MIL-101, constructed from Fe^{3+} ions and 1,4-benzenedicarboxylic acid (BDC) linkers, was reported to collapse under acidic conditions due to the protonation of carboxyl groups in BDC.[23] Although these materials show responsiveness under acidic conditions, they have been reported to remain considerably more stable in physiological environments. For instance, Xue and co-workers[24] described a doxorubicin (DOX)-loaded MIL-100 system that exhibited significantly higher drug release at pH 5.5 than at pH 7.4. After 60 h, the cumulative release under acidic conditions was more than twofold higher, indicating effective suppression of premature drug leakage at physiological pH. These features have motivated extensive investigation of such MOF families for drug delivery applications in cancer therapy.

2.2. Hypoxia

Hypoxia, a hallmark of the tumor microenvironment, arises from the rapid and uncontrolled proliferation of tumor cells that consume excessive amounts of oxygen, leading to severe oxygen deficiency within tumor tissues.[25] As previously reported, oxygen levels in the tumor microenvironment range from 0 to 2 mmHg, while in normal tissues they are in the range of 30–50 mmHg, representing a significant 25-fold decrease.[26] This condition markedly compromises the efficacy of several cancer therapies, particularly oxygen-dependent modalities such as PDT and RDT. Moreover, under hypoxic conditions, hypoxia-inducible factors (HIFs), primarily HIF-1α, are upregulated, which is associated with increased tumor metabolism and invasion, thereby contributing to drug resistance.[27] Owing to their versatility, several types of MOFs were designed to be responsive to the hypoxic tumor microenvironment. For example, Huang and co-workers[28] developed an azoreductase-responsive MOF system composed of Fe^{3+} and 4,4′-azobisbenzoic acid (AZO), in which the azobenzene units within the framework are reduced to amines by highly expressed azoreductase under hypoxic conditions, thereby inducing the release of the encapsulated cargo. In an *in vitro* MCF-7 cell model cultured under varying oxygen levels, western blot analysis demonstrated that even under severe hypoxia ($<1\%$ O_2), HIF-1α expression was significantly reduced compared with untreated normoxic controls ($<20\%$ O_2). These results indicate efficient system degradation in hypoxic environments, thereby supporting enhanced therapeutic efficacy of the delivered agents. In a similar trend, the Cu-MOF system proposed by Zhang *et al.*[29] exhibited hypoxia-responsive properties, thereby enhancing cancer therapy by augmenting both SDT and CDT. Moreover, MOFs can also effectively alleviate hypoxia either by delivering oxygen endogenously or by generating it exogenously through interactions with intracellular components, ultimately enhancing therapeutic efficacy.

2.3. Redox system

The rapid proliferation of tumor cells significantly increases their metabolic activity, which in turn leads to a sharp rise in reactive oxygen species (ROS). ROS are oxygen-containing free radicals that play dual roles in cellular regulation. At a proper threshold, ROS play a vital role in various physiological processes; however, at high levels, they may cause oxidative stress and trigger cell death. A typical example is hydrogen peroxide (H_2O_2), a byproduct of cellular metabolism, which is produced at much higher levels in cancer cells than in normal cells, reaching up to 0.5 nmol/10^4 cells per h.[25] Indeed, previous studies have shown that at concentrations as low

as 50 μM, H_2O_2 begins to inhibit cell growth, and when levels increase to 200–1000 μM, it can induce apoptosis.[30] In addition, H_2O_2 is a major precursor of highly reactive ROS, such as hydroxyl radicals, peroxynitrite, and hypochlorite, all of which can also induce cell death when they reach the appropriate concentration. To counteract the adverse effects caused by ROS, cancer cells have evolved potent antioxidant defense systems, with glutathione (GSH) serving as a pivotal regulator in scavenging excess ROS and maintaining intracellular redox homeostasis.[31] This shielding ability makes GSH indispensable for tumor progression and has been shown to exhibit pronounced upregulation in tumor cells. The intracellular GSH concentrations in cancer cells (2–10 mM) are demonstrated to be significantly higher than those in normal cells (2–20 μM), corresponding to an increase of approximately 2–4 orders of magnitude.[17] Such elevated GSH levels, however, also present a major barrier to ROS-based therapeutic strategies, such as chemotherapy (CT), CDT, PDT, *etc.*

In this context, MOFs represent a promising strategy to overcome the aforementioned challenges while simultaneously preserving or even enhancing the therapeutic efficacy of drug delivery systems. Notably, the metal ions incorporated into the MOF framework can deplete intracellular GSH, thereby weakening the antioxidant defenses of cancer cells and improving treatment outcomes. Furthermore, active ions such as Fe^{3+}, Cu^{2+}, and Co^{2+} can participate in Fenton or Fenton-like reactions, utilizing H_2O_2 as a substrate to generate highly cytotoxic hydroxyl radicals ($^{\bullet}OH$). It has been suggested that in the GSH-enriched tumor microenvironment (0.5–10 mM), MOFs may undergo disintegration, releasing metal ions that can subsequently participate in redox reactions to form highly active metal species.[32] For instance, Chatterjee and colleagues[33] developed a Cu-MOF system that functions as a self-sufficient agent for both CDT and CT. Given the complexity of the tumor microenvironment, certain MOFs have been designed to respond to multiple stimuli. In this context, the CuMOF system exhibited sensitivity to both GSH-enriched and mildly acidic conditions (GSH 15 mM, pH 6.1), undergoing near-complete degradation accompanied by the release of Cu^{2+} ions. With the incorporation of the H_2O_2 self-supplying agent CaO_2, the system further enabled efficient ROS generation, as confirmed by fluorescence probe analysis *in vitro*. These combined stimulus-responsive and catalytic behaviors translated into significantly enhanced antitumor efficacy, as evidenced by a greater reduction in tumor weight in tumor-bearing mice compared with conventional CT. Other strategies have also been proposed in recent years, involving not only the responsive behavior of metal ions but also the incorporation of stimuli-responsive linkers within the framework. A representative study by Yao and co-workers[34] designed an Fe-MOF incorporating GSH-responsive disulfide-bonded organic ligands to directly target GSH depletion. *In vitro* release studies showed significantly higher drug release in the presence of GSH, highlighting the synergistic pH–GSH dual-responsive mechanism in which acidic pH weakens Fe^{3+} coordination and GSH cleaves disulfide bonds, thereby accelerating MOF disintegration. Collectively, these mechanisms establish dual responsiveness within the system, ensuring therapeutic efficacy while eliminating the need for external stimuli, relying predominantly on the intrinsic properties of the MOF structure.

2.4. ATP

Adenosine triphosphate (ATP), referred to as the main energy currency of cells, is indispensable for a broad range of fundamental biological processes.[17] Intracellular ATP supports tumor cell growth, proliferation, and metabolic activity, whereas extracellular ATP functions as a signaling molecule that modulates immune cell recruitment and activation, thereby influencing antitumor immune responses.[35] In the tumor microenvironment, ATP is generated at markedly elevated levels to sustain the excessive metabolic demands of tumor cells. ATP concentrations in healthy tissues are typically confined to the nanomolar range of 10–100 nM, whereas tumor cells exhibit much higher extracellular concentrations, reaching 100–500 μM.[36] This pronounced disparity in ATP levels between tumor and normal tissues has driven extensive investigation into the design of ATP-responsive delivery systems for selective transport and release at target sites. Certain MOF structures are susceptible to cleavage in ATP-rich environments; for example, both ZIF-8 and ZIF-90 have been demonstrated to undergo disassembly under elevated ATP concentrations. Notably, ZIF-90 exhibits a greater tendency toward decomposition, largely due to differences in its organic ligands 2-imidazolecarboxaldehyde (2-ICA), which favor competitive coordination with ATP, thereby making it an attractive candidate for the design of MOFs with selective ATP-responsive properties.[37] For instance, Xu *et al.*[38] designed a Cu^{2+}-doped ZIF-90 system to selectively degrade in response to the high ATP levels of cancer cells. The degradation of Cu^{2+}-doped ZIF-90 was promoted upon exposure to ATP at varying concentrations (2–10 mM), resulting in the release of Cu^{2+} ions and therapeutic agents. Antitumor efficacy was further evaluated *in vivo*, where the synergistic activity of Cu^{2+} and the active agents mediated by an ATP-responsive mechanism led to a fivefold reduction in tumor volume compared with untreated groups after 14 days, while maintaining a survival rate above 0.6 at the end of treatment. Building on this concept, numerous MOF-based systems have since been developed to exploit ATP-responsive properties for the controlled delivery of therapeutic cargo.

2.5. Ions

Ion-exchange processes are frequently observed during the interaction of MOFs with physiological environments. Nevertheless, these mechanisms are rarely employed in isolation; instead, they are typically incorporated into more complex, integrated strategies, where ion-responsiveness functions synergistically with other mechanisms to optimize therapeutic performance. Within the tumor microenvironment, where multiple biological processes occur simultaneously, the accumulation of cations (*e.g.*, Ca^{2+}, K^{+}, Cu^{2+}, Zn^{2+}) and anions (*e.g.*, PO_4^{3-}, HPO_4^{2-}, $H_2PO_4^{-}$) has been suggested as a potential trigger for the development of MOF-based delivery systems.[39] Ion-exchange processes in this context can generally be categorized into two principal mechanisms: competitive binding and anion-exchange. First, competitive binding occurs when metal ions with higher binding affinity in

the tumor microenvironment displace lower-affinity ions within the MOF structure. This competition can take place both at the coordination sites of the framework and with the organic ligands, thereby inducing structural transformations and enabling stimulus-responsive drug release.[40] A representative example is the drug-loaded MOF-In system, proposed by Du *et al.*,[41] which exhibits enhanced drug loading and release behavior in the presence of Zn^{2+} as the competing ion due to the abundance of Zn^{2+} in brain extracellular fluid. Second, anion exchange is driven by the strong binding affinity of environmental anions toward the metal centers within the MOF framework.[42] Among these, phosphate ions are particularly important, as they are abundant in physiological environments and serve as integral components of ATP. The ATP-responsive disassembly of certain MOFs can, therefore, be directly linked to this anion-exchange process. Similarly, Miao and co-workers[42] proposed an Al-MOF system that demonstrated gradual disintegration in phosphate-containing simulated intracellular fluid, thereby enabling the controlled release of the encapsulated cargo. Although the threshold concentrations and spatial availability of individual metal ions and anions are not yet well defined in the existing literature, these observations suggest the feasibility of ion-mediated release mechanisms. Accordingly, such mechanisms are more suitably regarded as complementary components within integrated stimuli-responsive systems rather than as standalone selective triggers.

3. Applications of MOF-based drug delivery systems

Drug-based treatment, ranging from FDA-approved drugs to bioactive compounds with therapeutic potential, is one of the most common first lines of cancer therapy. However, these treatments often face significant challenges related to bioavailability, which serves as a critical determinant of therapeutic performance. Most chemotherapeutic agents (*e.g.*, docetaxel, paclitaxel, camptothecin) and bioactive compounds (*e.g.*, curcumin, quercetin, silymarin) are hydrophobic because of their abundant aromatic structures, and their low solubility restricts systemic circulation and absorption.[43,44] In contrast, hydrophilic drugs (*e.g.*, doxorubicin, cisplatin, 5-fluorouracil) exhibit high solubility and prolonged circulation but show low permeability and are more prone to enzymatic degradation and systemic clearance.[45] These factors often result in reduced drug bioavailability, necessitating repeated dosing and increasing the risk of systemic toxicity, which can lead to a wide range of adverse side effects in patients. MOFs, owing to their remarkable versatility and tunability during synthesis, represent a promising platform to overcome these challenges. With their porous architecture, high surface area, large void volume, and available functional groups for modification, MOFs can encapsulate diverse therapeutic agents and serve as multifunctional delivery systems, effectively addressing the limitations of conventional approaches and synergistically enhancing therapeutic efficacy, as demonstrated in Table 1.

The incorporation of drugs into MOF-based delivery systems has been shown to significantly enhance therapeutic efficacy, as demonstrated by numerous recent studies. For example, Xu and colleagues[46] employed the system of spiky nanosystem S@Cu-MOF, composed of Cu^{2+} and the ligand 1,3,5-benzenetricarboxylic acid (BTC), to encapsulate polyphyllin I (PPI), a promising anticancer agent limited by poor solubility (Fig. 1). As a delivery vehicle, S@Cu-MOF not only effectively encapsulated PPI but also enhanced its therapeutic efficacy through its unique spiky structure, which promoted cellular uptake and induced DNA damage. When combined with αPD-1, the S@Cu-MOF/PPI + αPD-1 treatment markedly suppressed tumor progression in 4T1 tumor-bearing mice, achieving a tumor inhibition rate of 76.2% after 8 days with 5 repeated doses. This efficacy was substantially higher than that of αPD-1 monotherapy (38%) and PPI treatment alone (25%) at equivalent doses. In addition to its pronounced antitumor activity, the material system exhibited a favorable safety profile, with no detectable systemic toxicity or organ damage. In another study, Wang and co-workers[47] developed a Zr-MOF, constructed from Zr^{4+} and 5,10,15,20-tetra(4-carboxyphenyl)porphyrin (TCPP), as a carrier to improve the therapeutic efficacy of DOX. In addition to its role as a drug carrier, Zr-MOF contributed to preventing the rapid clearance of therapeutic agents from tumor sites. *In vivo* retention studies using near-infrared fluorescence imaging of indocyanine green demonstrated that, while the free drug was rapidly cleared from the tumor within 48 h after administration, more than 25% of the drug-loaded Zr-MOF remained localized at the tumor site. This prolonged tumor retention of the MOF-based delivery system further enhanced antitumor efficacy, resulting in significantly lower tumor weights in CT-26 tumor-bearing mice compared with free DOX after 21 days of treatment. Moreover, owing to their intrinsic porous architectures, characterized by high surface area, large pore volume, and tunable pore size, many MOFs exhibit exceptional drug-loading capacities. For instance, Tan *et al.*[48] reported a Zr-MOF constructed with NH_2-BDC as ligands, which exhibited a surface area of 902.71 m2 g^{-1} and a pore volume of 0.34 cm^3 g^{-1}. Leveraging these structural advantages, the authors successfully co-loaded two therapeutic agents with distinct physicochemical properties, namely hydrophilic DOX and hydrophobic celecoxib (CEL). Despite employing a relatively high feeding ratio (5 mg Zr-MOF with 5 mg DOX and 2.8 mg CEL), the system achieved notably high loading capacities of 46.85 ± 3.26 wt% for DOX and 26.47 ± 3.46 wt% for CEL. These findings underscore the capability of MOFs to function not only as drug carriers but also as highly efficient delivery platforms that may help overcome limitations associated with conventional single-drug therapies.

In recent years, a novel class of MOFs, termed bio-MOFs, have been developed. These frameworks incorporate at least one biomolecule as an organic ligand to improve biological performance. Within this concept, an emerging strategy is the direct use of drugs as ligands to construct bio-MOFs, thereby integrating therapeutic functionality into the framework itself. Although bio-MOFs often exhibit lower porosity than conventional MOFs, as the functional groups within their ligands may limit framework coordination, they provide notable advantages

Table 1 Applications of MOF-based drug delivery systems for cancer therapy

Delivery system	Cargo	MOF components	Stimuli	*In vitro*	*In vivo*	Application	Ref.
Cu-GA/DOX@ZIF-8	DOX	Zn^{2+}, 2-MIM	pH	C26	—	Anticancer by CT	22
Cu-TA/CUR@ZIF-8	CUR	Zn^{2+}, 2-MIM	pH	C26	—	Anticancer by CT	52
FeTPt@CCM	Pt(IV)–$(COOH)_2$	Fe^{3+}, TCPP	pH, GSH	4T1	4T1 tumor-bearing BALB/C mice	Anticancer by combined CT and CDT	53
DSF@MOF-199@FA	DSF	Cu^{2+}, BTC	pH	SW480, HeLa, 4T1	4T1 tumor-bearing BALB/C nude mice	Anticancer by enhanced CT	54
CaO_2@DOX@ZIF-67	DOX	Co^{2+}, 2-MIM	pH	MCF-7	MCF-7 tumor-bearing Nu/Nu nude mice	Anticancer by combined CT and CDT	55
ATV@FM@PMPC	ATV	Fe^{3+}, BDC	pH, GSH	CT-26, MCF-7, Hepa1–6, A549	CT-26 tumor-bearing BALB/C mice and ICR mice	Anticancer by enhanced CDT	56
ORL@Cu-MOF	ORL	Cu^{2+}, BTC	pH, GSH	SCC-9, Cal-27, MOC-2	MOC-2 tumor-bearing C57/BL6 mice	Anticancer by combined CDT and IT	57
S@Cu-MOF/PPI	PPI	Cu^{2+}, BTC	Intracellular environment	4T1	4T1 tumor-bearing BALB/C mice	Anticancer by inducing cuproptosis and enhanced IT	46
DOX@Zr-MOF	DOX	Zr^{4+}, TCPP	pH	CT26, SH-SY5Y	CT26 tumor-bearing BALB/C mice	Anticancer by combined CT and IT	47
DOX/CEL/MOF	DOX CEL	Zr^{4+}, NH_2-BDC	pH	A549, KB, HepG2, SCC-9	SCC-9 tumor-bearing BALB/C nude mice	Anticancer by enhanced CT	48
UIO-66-Let/Epi@NH_2	Let Epi	Zr^{4+}, NH_2-BDC	pH	MCF-7	—	Anticancer by enhanced CT	58
CDDP@UiO@-DOX@poly(*ortho* ester) NP (CUDPOE)	CDPP DOX	Zr^{4+}, NH_2-BDC	pH	4T1, MCF/ADR, HepG2	MCF-7/ADR tumor-bearing nude mice	Anticancer by enhanced CT	59
CUR-BMS1166@ZIF-8@PEG-FA (CBZP)	CUR BMS1166	Zn^{2+}, 2-MIM	pH	K7M2	K7M2 tumor-bearing BALB/C mice	Anticancer by enhanced IT	60
DOX@Zn-cys bio-MOF/FC	DOX	Zn^{2+}, L-cystine	pH, GSH	MCF-7	—	Anticancer by CT	61
Apt-PEG-MOF@DOX	CUR DOX	Fe^{2+}, CUR	pH	HT-29	HT-29 tumor-bearing C57BL/6 mice	Anticancer by enhanced CT	50
MPDH	CUR DOX	Zn^{2+}, CUR	pH, NIR laser irradiation	HeLa	—	Anticancer by combined CT and CDT	51
DOX@ZIF-8-on-ZIF-8 (DZZ)	DOX	Zn^{2+}, 2-MIM	pH, GSH	4T1	4T1 tumor-bearing BALB/C nude mice	Anticancer by enhanced CT	62
DOX@NH_2-MIL-88B-On-NH_2-MIL-88B (DMM)	DOX	Fe^{3+}, NH_2-BDC	pH, GSH	4T1	—	Anticancer by combined CT and CDT	63
PCN@DOX/ZIF	DOX	Zr^{4+}, TCPP; Zn^{2+}, 2-MIM	pH, visible laser irradiation	4T1 MCF-7	4T1 tumor-bearing BALB/C mice	Anticancer by combined CT and PDT	64
(DOX and ICG)@H-PMOF@mem (DIHPm)	DOX	Zn^{2+}, 2-MIM; Zr^{4+}, TCPP	pH, visible and NIR laser irradiation	4T1, U87MG, A549	4T1 tumor-bearing BALB/C mice	Anticancer by combined CT, PTT and PDT	65

Note: DOX: doxorubicin; CUR: curcumin; Pt(IV)–$(COOH)_2$: dihydroxyl oxaliplatin prodrug; DSF: disulfiram; ATV: atorvastatin; ORL: orlistat; PPI: polyphyllin I; CEL: celecoxib; Let: letrozole; Epi: epirucin; CDPP: cisplatin; ICG: indocyanine green; 2-MIM: 2-methylimidazole; TCPP: 5,10,15,20-tetra(4-carboxyphenyl)porphyrin; BTC: 1,3,5-benzenetricarboxylic acid; BDC: 1,4-benzenedicarboxylic acid; 2-ICA: 2-imidazolecarboxaldehyde; H_4TBAPy: 1,3,6,8-tetrakis(*p*-benzoic acid)pyrene; TpyP: 5,10,15,20-tetrakis(4-pyridyl)-21*H*,23*H*-porphine; DTA: 5,5-dimethyl-4,6-dithia-nonanedioic acid; CT: chemotherapy; CDT: chemodynamic therapy; RT: radiotherapy; RDT: radiodynamic therapy; SDT: sonodynamic therapy; PTT: photothermal therapy; PDT: photodynamic therapy; XDT: X-ray-induced dynamic therapy; IT: immunotherapy.

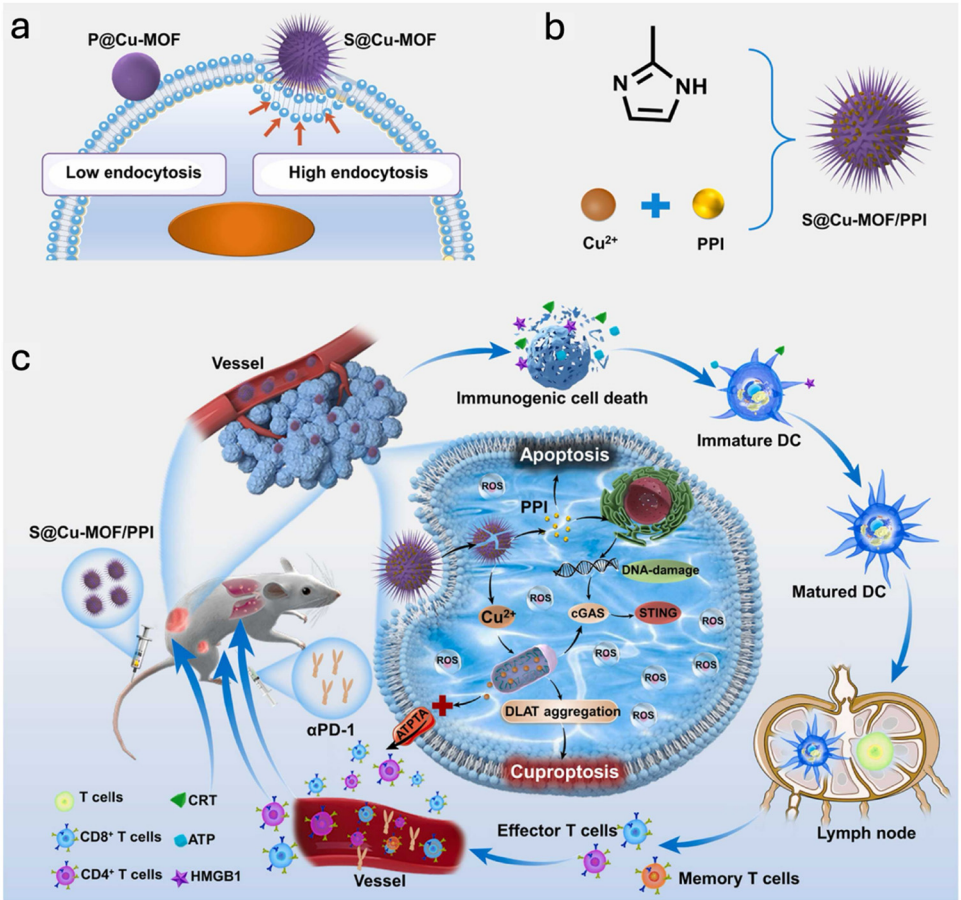

Fig. 1 The design and anticancer mechanism of the S@Cu-MOF/PPI system for enhanced IT. (a) Comparative analysis of plain and spiky nanoparticles demonstrating shape-dependent cellular uptake. (b) Schematic representation of S@Cu-MOF/PPI preparation. (c) Mechanistic pathway illustrating Cu^{2+} release, mitochondrial disruption, induction of cuproptosis, and activation of the cyclic GMP–AMP synthase-stimulator of interferon genes (cGAS/STING) pathway, collectively sensitizing tumors to αPD-1 therapy and resulting in tumor suppression, metastasis inhibition, and immune memory induction. This figure has been reproduced from ref. 46 with permission from Elsevier, copyright 2024.

in biocompatibility and can harness the inherent therapeutic activity of bio-derived ligands.[49] For instance, Babaei *et al.*[50] constructed a bio-MOF using curcumin (CUR) as the organic ligand to coordinate with Fe^{3+}. This bio-MOF allowed the post-loading of an additional therapeutic agent, DOX, achieving a high loading capacity (39.0 ± 1.4 wt%) and encapsulation efficiency (92.3 ± 2.2%) at a material-to-drug feeding ratio of 1 : 1. Notably, under favorable conditions, the CUR ligands incorporated into the framework could be released concurrently with the loaded DOX, enabling the simultaneous delivery of both therapeutic agents. With the same concept, Yang and colleagues[51] developed a CUR-Zn^{2+} bio-MOF, to enhance the therapeutic efficacy besides the anticancer effect of DOX. Under acidic conditions and NIR stimulation, the system enabled the coordinated release of both drugs, achieving up to 19.15 μg of CUR per 1 mg of nanocarrier and approximately 60.83% release of DOX after 1400 min. The effectiveness of this approach was further reflected in *in vitro* cytotoxicity studies using HeLa cells, where the dual-drug delivery system exhibited a lower IC_{50} value (0.254 mg mL^{-1}) compared with DOX alone (0.341 mg mL^{-1}). These findings support the versatility of MOF-based platforms for combination drug delivery and provide a basis for further investigations into MOF structural engineering using therapeutic molecules to enable multi-drug targeting strategies.

4. Applications of MOF-based nucleic acid delivery systems

In recent decades, advances in science and technology have facilitated the development of novel cancer therapies, with gene therapy receiving considerable attention. This strategy focuses on the delivery of nucleic acids into targeted tumor cells, where they can exert anticancer effects by modulating gene expression and biological functions.[66] Traditionally, viral vectors have been the primary vehicles for genetic material delivery. Although effective, as demonstrated in vaccine applications, their application is hindered by major drawbacks such as high immunogenicity, limited cargo capacity, potential pathogenicity, and high production costs.[67,68] As a result, non-viral vectors have been actively investigated as safe and versatile alternatives. Nevertheless, the

Table 2 Applications of MOF-based nucleic acid delivery systems for cancer therapy

Delivery system	Cargo	MOF components	Stimuli	*In vitro*	*In vivo*	Application	Ref.
pDNA@ZIF	pDNA	Zn^{2+}, 2-MIM	pH	PC-3	—	Anticancer potential by gene transfection	72
ZIF-90@Ce6-G3139/Ce6-DNAzyme	G3139 DNAzyme	Zn^{2+}, 2-ICA	pH, visible laser irradiation	MCF-7	—	Anticancer by combined gene therapy and PDT	79
Ce6/DNAzyme@ZIF-8	DNAzyme	Zn^{2+}, 2-MIM	pH, NIR laser irradiation	MCF-7	MCF-7 tumor-bearing BALB/C nude mice	Anticancer by combined gene therapy and PDT	73
DNAzyme@Cu/ZIF-8	DNAzyme	Zn^{2+}, 2-MIM	pH	MCF-7	MCF tumor-bearing BALB/C nude mice	Anticancer by gene therapy	80
Ce6-DNAzyme@ZIF-8@PEG (CDZP)	DNAzyme	Zn^{2+}, 2-MIM	pH, visible laser irradiation	4T1	4T1 tumor-bearing BALB/C mice	Anticancer by combined gene therapy and PDT	74
cRGD–PEI–DNAzyme@Mn/Zn-IP6	DNAzyme	Zn^{2+}, 2-MIM	pH	MCF-7	MCF-7 tumor-bearing BALB/C nude mice	Anticancer by high-efficiency gene therapy	75
Cancer membrane/siRNA@ZIF-8	Plk1 siRNA	Zn^{2+}, 2-MIM	pH	HeLa	HeLa tumor-bearing BALB/C nude mice	Anticancer by gene therapy	77
siRNA@nNU-1000	siRNA	Zr^{4+}, H_4TBAPy	pH	HEK293-mC	—	Anticancer potential by gene knockdown	78
FA-siPKM2-MnO_2-MOF	siPKM2	Zn^{2+}, 2-MIM	pH	MDA-MB-231, MCF-7, T47D	MDA-MB-231 tumor-bearing BALB/C nude mice	Anticancer by gene therapy	81
PCN@HCR	HCR probe	Zr^{4+}, TCPP	pH, visible laser irradiation	MCF-7	MCF-7 tumor-bearing BALB/C nude mice	Anticancer by combined gene therapy and PDT	82
NMOF-CS-FA-LNA-antisense miR-224 (MCFL224)	LNA-antisense miR-224	Zn^{2+}, BDC	pH	HCT116	—	Anticancer by gene therapy	83

Note: pDNA: plasmid DNA; G3139: oblimersen; siRNA: small interfering RNA; siPKM2: siRNA against pyruvate kinase muscle isozyme M2; HCR: DNA-based hybridization chain reaction; LNA: locked nucleic acid.

diversity in nucleic acid size and structure, coupled with their intrinsic fragility, presents significant challenges for delivery system design. Within this context, MOFs have emerged as particularly promising carriers. Their highly porous and tunable architectures enable efficient encapsulation of diverse nucleic acids while simultaneously providing protective shielding, thereby enhancing molecular stability and therapeutic efficacy. In addition to serving as effective carriers, MOFs can also synergistically enhance the activity of genetic materials, as summarized in Table 2.

For nucleic acid delivery, ZIF-8 has been predominantly employed compared to other types of MOFs, due to its ability to be synthesized under mild conditions that preserve the integrity of these fragile biomolecules.[69] Indeed, ZIF-8 can be rapidly fabricated at the nanoscale in aqueous environments and at room temperature, thereby minimizing potential degradation from harsh solvents, elevated temperatures, or prolonged reaction times.[70] Furthermore, its low *in vitro* and *in vivo* toxicity underscores its suitability for nucleic acid delivery in biomedical applications, which has led to extensive investigation in numerous studies.[71] Notably, ZIF-8 has demonstrated a remarkable capacity to carry large molecules, such as plasmid DNA (pDNA). In the study by Polash and colleagues,[72] ZIF-8 was synthesized under mild conditions by adding triethylamine to control the size of the composites. The results confirmed the successful formation of pDNA@ZIF-8 at the nanoscale, with more than 80% of the added pDNA encapsulated. This efficient encapsulation is attributed to the one-pot synthesis approach, which enables the structural tunability of ZIF-8 to accommodate pDNA. The pDNA encoded the green fluorescent protein, whose expression by the cellular machinery serves as an indicator of successful transfection. Following release from the pDNA@ZIF-8 system, the pDNA was successfully transfected into PC-3 cells, as evidenced by the observed green fluorescence. These results demonstrate the ability of ZIF-8 to effectively encapsulate and protect the bioactivity of pDNA during delivery. Moreover, Zn^{2+} ions released from the structure of ZIF-8 may function as critical cofactors for DNAzymes, enabling these single-stranded DNA molecules to selectively catalyze the cleavage of oncogenic RNA or DNA sequences, thereby inhibiting tumor progression.[73] For instance, Yang *et al.*[74] reported the use of ZIF-8 as an efficient carrier for GPX4–DNAzyme in breast cancer therapy. Following cellular internalization, the pH-responsive framework disassembled in the cancer cell cytoplasm, releasing DNAzyme and Zn^{2+} ions. The released Zn^{2+} activated the catalytic activity of GPX4–DNAzyme, leading to the suppression of GPX4 protein expression and impairing cellular ROS scavenging. The system was shown to be efficiently internalized and localized within the cytoplasm of MCF-7 cells within 8 h. Consistent with these *in vitro* findings, it demonstrated effective tumor accumulation 4 h after intravenous administration and achieved a tumor inhibition rate of 72.3% in tumor-bearing mouse models compared with the untreated group. Importantly, the platform also exhibited favorable *in vivo* safety, with no observable systemic toxicity or organ accumulation, and was cleared from the body within approximately 4 days. In addition to acting as a Zn^{2+} reservoir, the ZIF-8 structure can allow metal ion exchange, enabling the construction of MOF carriers containing multiple

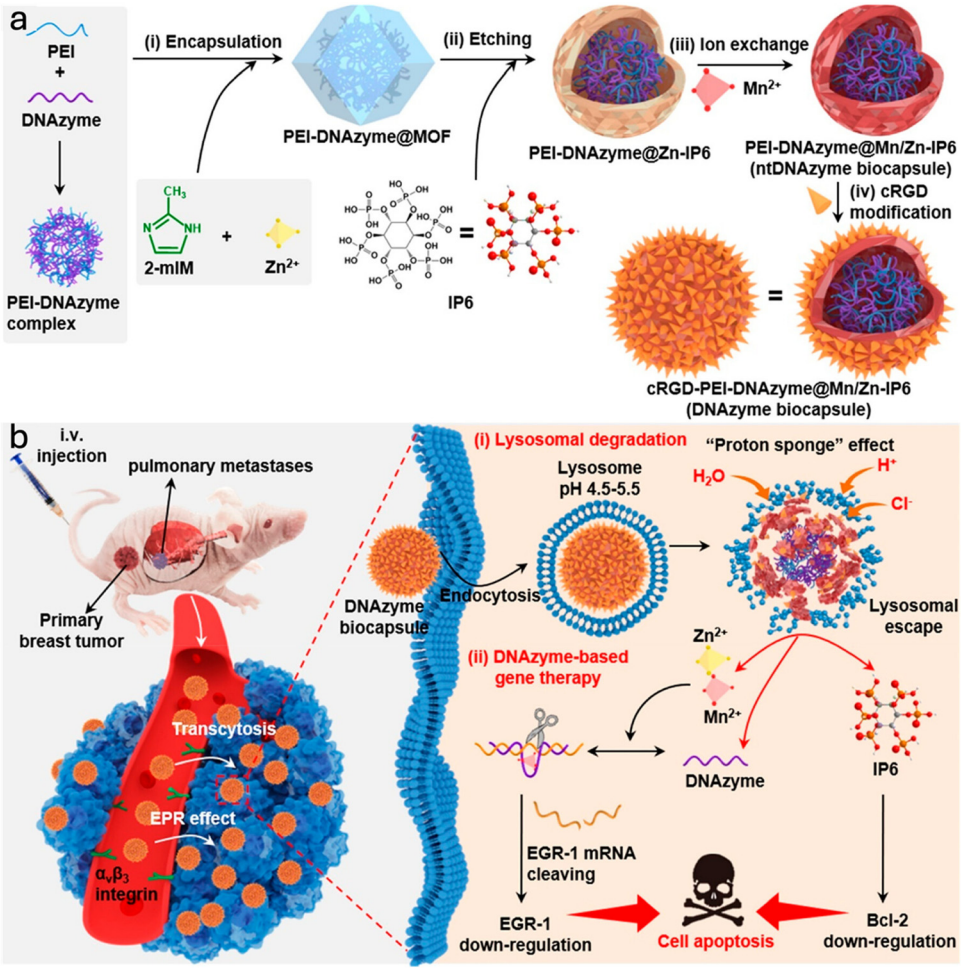

Fig. 2 The preparation and anticancer mechanism of degradable biomimetic DNAzyme nanocapsule (DNAzyme biocapsule)-mediated gene therapy for metastatic breast cancer. (a) The synthesis of the DNAzyme biocapsule from a PEI–DNAzyme complex within ZIF-8 MOFs *via* one-step biomimetic mineralization, followed by etching, ion exchange, and functionalization for enhanced targeting. (b) Mechanism of action in the intracellular environment, including tumor-specific accumulation, lysosomal degradation, and DNAzyme-mediated gene cleavage leading to cancer cell apoptosis. This figure has been reproduced from ref. 75 with permission from American Chemical Society, copyright 2023.

active metal species. Jiang and co-workers[75] developed an advanced system capable of self-supplying high concentrations of Mn^{2+}/Zn^{2+} dual cofactors to enhance DNAzyme-mediated cleavage of EGR-1 mRNA (Fig. 2). In brief, the system was fabricated *via* one-pot biomimetic mineralization of ZIF-8 onto PEI–DNAzyme, followed by IP6-assisted chemical etching to partially substitute framework Zn^{2+} with Mn^{2+}. The resulting platform achieved efficient DNAzyme encapsulation and exhibited pH-responsive release of DNAzyme and Mn^{2+}/Zn^{2+} ions under lysosome-mimicking conditions (pH 5.0). Importantly, given that functional preservation remains a major challenge in DNAzyme delivery, the material facilitated effective lysosomal escape by utilizing the ''proton-sponge'' effect of PEI. Fluorescence imaging studies demonstrated lysosomal escape as early as 3 h post-internalization, followed by cytosolic diffusion at 9 h, supporting the intracellular stability of the DNAzyme.

Small interfering RNA (siRNA) has also been effectively delivered using MOFs, where it binds to the framework through electrostatic interactions and multiple coordination bonds, while the MOF protects it from nuclease degradation.[76] For example, Zhang and colleagues[77] demonstrated that ZIF-8, with its large surface area (2012.728 $m^2\ g^{-1}$), pore volume (1.25 $cm^3\ g^{-1}$), and pore diameter (3.13 nm), enabled exceptionally high siRNA encapsulation efficiency (>99.9%). However, effective siRNA delivery requires not only efficient cellular internalization but also successful endosomal escape and subsequent release into the cytosol to activate gene-silencing pathways. These concerns were comprehensively investigated by Teplensky and co-workers.[78] They developed a nanoscale Zr-MOF, nNU-1000, with 3 nm hexagonal mesoporous channels, to enable high siRNA loading (150 pmol mg^{-1}) and protect the encapsulated siRNA from enzymatic degradation. Although siRNA@nNU-1000 exhibited superior cellular uptake in HEK293-mC cells compared to lipofectamine-mediated delivery, it did not result in enhanced gene-knockdown efficiency *in vitro*. Subsequent studies demonstrated that incorporation of endosomal escape-promoting cofactors effectively assisted siRNA@nNU-1000 to overcome endosomal retention and enabled effective gene-knockdown capabilities. Collectively, these findings

highlight the advantages of MOFs as high-capacity and protective nucleic acid carriers, while emphasizing the necessity of integrating advanced delivery strategies to address biological barriers arising from the labile nature of nucleic acids.

5. Applications of MOF-based protein delivery systems

Proteins are essential biomolecules that form the foundation of cellular structures and participate in diverse biological processes, serving as enzymes, antibodies, and cytokines.[84] Depending on their specific roles, protein delivery has attracted considerable attention for treating various diseases associated with altered intracellular proteins. This strategy offers unique therapeutic advantages, including high bioactivity and specificity.[85] However, protein-based cancer therapies face significant challenges, including proteolytic degradation, denaturation, short systemic half-life, instability during formulation, and inefficient intracellular transport due to their large molecular size compared to other biomolecules.[86,87] MOFs, in this case, have emerged as a promising carrier to address these limitations. By carrying proteins, MOFs protect them from the harsh conditions of the intracellular environment, facilitate targeted delivery, and enable controlled release in response to tumor microenvironment stimuli. Moreover, owing to their tunable synthesis, large protein molecules can be encapsulated within the MOF structure through one-pot synthesis, effectively utilizing the large void space to protect the cargo and address challenges associated with protein size (Table 3).

Glucose oxidase (GOx), an enzyme that catalyzes glucose into gluconic acid and H_2O_2, deprives tumor cells of their primary energy source, thereby having an anticancer effect through starvation therapy.[88] Incorporating GOx into MOFs provides additional advantages, as the metal ion nodes can participate in Fenton or Fenton-like reactions with intracellular components. This synergizes with the H_2O_2 generated by GOx, further amplifying ROS accumulation and ultimately inducing apoptosis. To illustrate, Shao and colleagues[89] developed a multi-responsive Cu-MOF system to deliver GOx for activating cancer cell pyroptosis. The overexpression of reductase in cancer cells triggered the reduction of the AZO ligand within Cu-MOF, leading to the release of Cu^{2+} and GOx. Under the intracellular GSH levels in cancer cells, Cu^{2+} was reduced into Cu^{+} and cooperated with the H_2O_2 generated by GOx to drive a Fenton-like reaction. Following intravenous administration, Cy3-labeled GOx@Cu-MOF exhibited appreciable accumulation at tumor sites within 6 h, whereas Cy3-GOx administered at an equivalent dose showed no detectable tumor localization in HeLa tumor-bearing models. Consistent with this biodistribution profile, GOx@Cu-MOF treatment

Table 3 Applications of MOF-based protein delivery systems for cancer therapy

Delivery system	Cargo	MOF components	Stimuli	*In vitro*	*In vivo*	Application	Ref.
GOx@Cu-MOF	GOx	Cu^{2+}, AZO	Intracellular reductase, GSH	HeLa	HeLa tumor-bearing BALB/C nude mice	Anticancer by CDT and cell pyroptosis	89
Anti-VEGFR2/GOx/Fe-MOF (MGaV)	GOx	Fe^{3+}, BTC	pH	A549, LN229 Huh-7	A549 tumor-bearing BALB/C nude mice	Anticancer by CDT, anti-angiogenesis and cancer starvation therapy	90
CHC/GOx@ZIF-8	GOx	Zn^{2+}, 2-MIM	pH	MCF-7, SiHa	SiHa tumor-bearing BALB/C nude mice	Anticancer by cancer starvation therapy	92
Co-Fc@GOx	GOx	Co^{2+}, FC	pH	4T1	4T1 tumor-bearing BALB/C mice	Anticancer by CDT	91
ZANP	OVA	Zn^{2+}, 2-MIM	pH	EG7-OVA	EG7-OVA tumor-bearing C57BL/6 mice	Anticancer by IT	96
SOM-ZIF-8/OVA	OVA	Zn^{2+}, 2-MIM	pH	—	B16-OVA tumor-bearing C57BL/6 mice	Anticancer by IT	97
OVA@HZIF-Mn	OVA	Zn^{2+}, 2-MIM	pH	—	B16F10-OVA tumor bearing C57BL/6 mice	Anticancer by enhanced IT	93
COD-MOF	COD	Zr^{4+}, BPYDC	pH	MCF-7/ADR, MCF-7, HepG2 4T1	MCF-7/ADR tumor-bearing BALB/C nude mice	Anticancer by catalyzing metabolic oxidation	98
TYR@NPCN-333	TYR	Al^{3+}, TATB	pH	SKOV3-TR, H1299, HeLa	HeLa tumor-bearing BALB/C nude mice	Anticancer by inducing apoptosis	95
MCM@UN	NHWD-870	Zr^{4+}, BDC	pH	4T1	4T1 tumor-bearing BALB/C mice	Anticancer by IT	99
MOF-protein (MP)	Protein (BSA, Cyt *c*, gelonin)	Zn^{2+}, 2-MIM	pH	MDA-MB-231	MDA-MB-231 tumor-bearing BALB/C nude mice	Anticancer by effective delivery	94
Ce6/Cyt *c*@ZIF-8/HA	Cyt *c*	Zn^{2+}, 2-MIM	pH	HeLa, SMMC7721	HeLa tumor-bearing BALB/C mice	Anticancer by combined PDT and protein therapy to enhance apoptosis	100
RCA template/protein@ZIF-8@Cu (PZCT)	BSA, ϕ29DP	Zn^{2+}, 2-MIM	pH, GSH	MCF-7	MCF-7 tumor-bearing BALB/C mice	Anticancer by combined gene therapy and CDT	101

Note: GOx: glucose oxidase; OVA: ovalbumin; COD: cholesterol oxidase; TYR: tyrosinase; NHWD-870: BET family bromodomain inhibitor with selectivity for BRD4; BSA: bovine serum albumin; Cyt *c*: cytochrome *c*; ϕ29DP: ϕ29 DNA polymerase; BPYDC: 2,2′-bipyridine-4,4′-dicarboxylic acid; TATB: 4,4′,4″-*s*-triazine-2,4,6-triyl-tribenzoic acid; FC: 1,1′-ferrocenedicarboxylic acid; AZO: 4,4′-azobisbenzoic acid.

resulted in a significantly enhanced antitumor response, yielding an approximately 9-fold reduction in tumor volume after 16 days compared with free GOx. These findings indicate that MOF-based delivery systems can effectively improve tumor accumulation and therapeutic performance of protein-based agents. Similar patterns were observed in other studies, where Fe^{3+} present within the MOF structure, either as metal nodes or incorporated in the ligands, was shown to synergize with the therapeutic efficacy of GOx against cancer.[90,91] In contrast to Cu-MOFs or Fe-MOFs, which actively participate in Fenton or Fenton-like reactions, MOFs containing inactive ions such as Zn^{2+} can assume alternative roles. For instance, Yu and co-workers[92] employed ZIF-8, where Zn^{2+} metal sites facilitated the co-loading of GOx and α-cyano-4-hydroxycinnamate (CHC), a lactate dehydrogenase inhibitor that deprives tumor cells of lactate, an additional energy source besides glucose. Using a one-pot synthesis strategy, CHC (2.5 wt%) and GOx (11.9 wt%) were efficiently co-encapsulated, and GOx preserved catalytic activity comparable to the free enzyme after incorporation into ZIF-8. Moreover, rapid cellular internalization of CHC/GOx@ZIF-8 was observed within 20 min of incubation, which in turn facilitated enhanced intracellular ROS generation and strengthened the therapeutic outcome of starvation-based therapy.

Several other proteins with anticancer potential have also been investigated using MOFs as carriers. For example, Cheng *et al.*[94] demonstrated that ZIF-8 can encapsulate a wide variety of proteins with a loading capacity of up to 41.0 wt%, while maintaining nanoscale sizes in the 50–100 nm range, as confirmed by TEM and SEM. Furthermore, its characteristic pore aperture of 1 nm effectively prevents proteolytic enzymes (2–10 nm) from penetrating the framework, thereby providing a protective "shelter" for the encapsulated proteins. In another study by Zhao and co-workers,[93] ovalbumin (OVA), an antigen capable of stimulating an immune response against tumor cells, was encapsulated within ZIF-8 with Mn^{2+} ions serving as an adjuvant (Fig. 3). OVA was fluorescently labeled with FITC to evaluate its intracellular localization. While FTIC-OVA predominantly accumulated in lysosomes, FITC-OVA@HZIF-Mn exhibited efficient lysosomal escape and cytosolic distribution. These MOF-assisted intracellular trafficking features contribute to the preservation of antigen activity and subsequently enhance antitumor efficacy through improved immunotherapeutic performance. Demonstrating the structural versatility of MOFs, Lian and co-workers[95] developed an enzyme-MOF nanoreactor using PCN-333, composed of Al^{3+} and 4,4′,4″-*s*-triazine-2,4,6-triyl-tribenzoic acid (TATB) ligands. With its hierarchical microporous (1.5 nm)

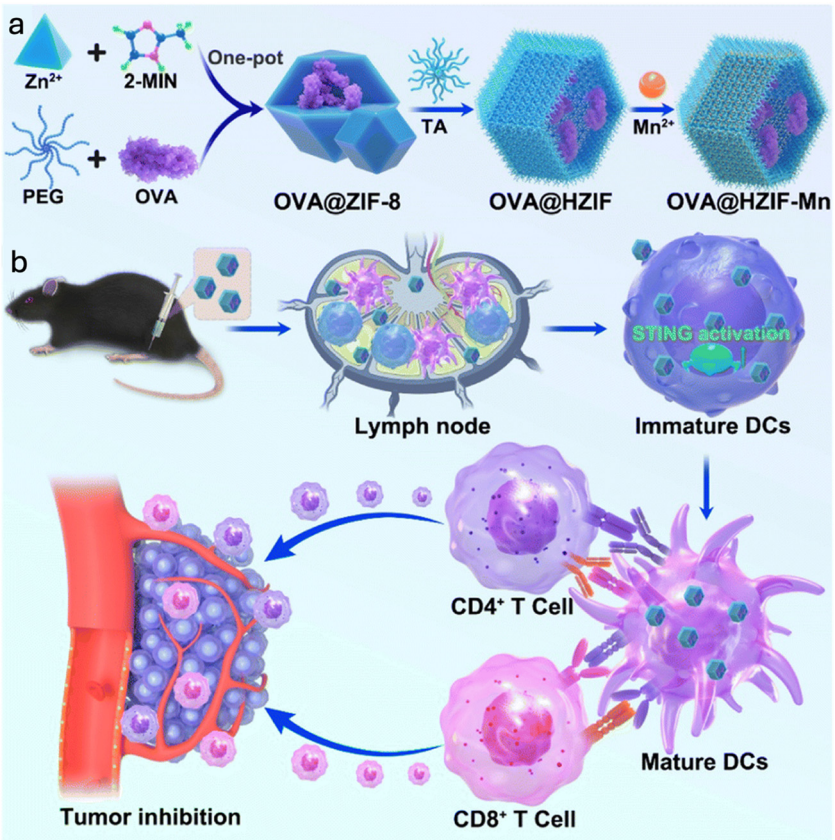

Fig. 3 The synthesis and antitumor properties of OVA@HZIF-8-Mn in activating tumor IT. (a) Fabrication of OVA@HZIF-8-Mn *via* a one-pot synthesis followed by surface modification for system optimization. (b) *In vivo* activity of OVA@HZIF-8-Mn after intravenous administration, demonstrating activation of the STING pathway for effective tumor therapy. This figure has been reproduced from ref. 93 with permission from Royal Society of Chemistry, copyright 2024.

and macroporous (4.2 and 5.5 nm) cages, PCN-333 efficiently accommodated tyrosinase (TYR) with a high loading capacity of 80 wt%. PCN-333 not only protected TYR from proteolytic degradation but also achieved 2.5-fold tumor regression after a single treatment, underscoring the potential of MOFs as versatile carriers capable of delivering a wide range of therapeutic payloads for cancer therapy.

6. Applications of MOF-based gas delivery systems

Gas therapy involves the use of therapeutic gases such as oxygen (O_2), nitric oxide (NO), carbon monoxide (CO), hydrogen sulfide (H_2S), and hydrogen (H_2), which have all shown potential in cancer treatment.[102] Within the tumor microenvironment, these gases regulate signal transduction, influence cancer cell functions, and hinder other cancer therapies. Their therapeutic outcomes, however, are highly dependent on concentration and exposure time: low doses may promote tumor growth, while high concentrations or prolonged exposure can suppress tumor progression through various mechanisms.[103] The major challenge of gas therapy lies in the short half-lives of these molecules and their site-specific, concentration-dependent bioactivities, necessitating advanced delivery systems for controlled release.[104] MOFs, with the advances in their porous structure, have emerged as ideal carriers. In brief, MOFs deliver gases to target sites mainly through two mechanisms: (i) catalytic (indirect delivery) and (ii) non-catalytic (direct delivery) (Table 4).

Among therapeutic gases, NO, H_2S, and CO are important signaling molecules that exhibit both direct and indirect antitumor effects (*e.g.*, induce apoptosis, immunomodulation, ferroptosis).[103] Their therapeutic concentrations typically fall within the nanomolar to micromolar range, where elevated levels exert anticancer effects by inhibiting mitochondrial respiratory metabolism.[105] As NO, H_2S, and CO exhibit concentration-dependent activities, controlled release of these biological gases is a primary concern for delivery systems to enhance therapeutic performance while avoiding blood poisoning due to off-target exposure.[102,104] These gas molecules are typically delivered indirectly in the form of gas donors or gas-releasing molecules, where exposure to specific stimuli can facilitate gas release. Accordingly, gas therapy is often integrated with other therapeutic modalities, such as PDT, PTT, and RDT, to achieve two primary objectives: (i) stimulus-responsive controlled gas release and (ii) synergistic antitumor effects.[106] In this context, highly porous porphyrin-based MOFs are particularly advantageous, as they not only enable efficient gas delivery but also demonstrate enhanced PDT and PTT through their responsiveness to external stimuli.[107] For instance, Zhang *et al.*[108] developed a porphyrin-based NMOF (Zr^{4+}/Mn-TCPP) to encapsulate *S*-nitrosothiol (SNO), a type of NO donor. The nanoscale spindle-shaped NMOF enabled efficient SNO loading with a capacity of 25.43 wt%, as confirmed by thermogravimetric analysis. The results indicated that, in the absence of laser irradiation, only a negligible amount of NO was released. In contrast, upon 808 nm laser irradiation, the photothermal effect of the NMOFs induced a localized temperature increase, leading to cleavage of the S–NO bond and thereby enabling controlled NO release (>25 μM within 80 min). In another study, Cao *et al.*[109] developed a PMOF composed of high atomic number elements Hf^{4+} and TCPP for delivering the dual-gas donor thio-3-hydroxyflavone (SHF) (Fig. 4). Upon X-ray irradiation, SHF@PMOF simultaneously released CO (up to 14 μM) and H_2S (up to 8 μM) in a controlled manner, while the PMOF itself generated ROS through the activities of Hf^{4+} and TCPP. Both SHF@PMOF and PMOF exhibited negligible cytotoxicity toward 4T1 cells in

Table 4 Applications of MOF-based gas delivery systems for cancer therapy

Delivery system	Cargo	MOF components	Stimuli	*In vitro*	*In vivo*	Application	Ref.
GSNO/Ce6@ZIF-8	GSNO	Zn^{2+}, 2-MIM	pH, ultrasound irradiation	MDA-MB-231, 4T1	4T1 tumor-bearing BALB/C mice	Anticancer by combined gas therapy and SDT	114
NMOF-SNO	SNO	Zr^{4+}, Mn-TCPP	NIR irradiation	MCF-7	MCF-7 tumor-bearing BALB/C nude mice	Anticancer by combined gas therapy and PTT	108
L-Arg@PCN@Mem	L-Arg	Zr^{4+}, TCPP	NIR irradiation	4T1, CT26	4T1 tumor-bearing BALB/C mice	Anticancer by combined gas therapy and PDT	115
MCM@PEG-CO	MnCO	Fe^{3+}, BTC	NIR irradiation	HCT116	HCT116 tumor-bearing nude mice	Anticancer by combined gas therapy and PTT	116
ZrRuMn-MONs@mem	MnCO	Zr^{4+}, Ru^{2+}, BPYDC	X-ray irradiation	HepG2	HepG2 tumor-bearing BALB/C nude mice	Anticancer by combined gas therapy and XDT	117
MnCO@Ti-MOF	MnCO	Ti^{4+}, BPYDC	Intracellular H_2O_2	HeLa, AGS	—	Anticancer by gas therapy	110
MnCO@UiO-67-bpy	MnCO	Zr^{4+}, BPYDC	Intracellular H_2O_2	HeLa, MCF-7	HeLa tumor-bearing BALB/C nude mice	Anticancer by combined gas therapy and CDT	118
SHF@PMOF	SHF	Hf^{4+}, TCPP	X-ray irradiation	4T1	4T1 tumor-bearing BALB/C mice	Anticancer by gas therapy, RT and RDT	109
PdH-MOF	H_2	Pd^{2+}, TPyP	NIR irradiation	4T1	4T1 tumor-bearing BALB/C mice	Anticancer by combined gas therapy and PTT	113
CuTz-1-O_2@F127	O_2	Cu^{+}, 3,5-Ph2-tzH	NIR irradiation	HeLa, 4T1	4T1 tumor-bearing BALB/C mice	Anticancer by combined gas therapy and PDT	111
O_2-loaded PMPP (PMPPO)	O_2	Ti^{4+}, NH_2-BDC	Ultrasound irradiation	4T1	4T1 tumor-bearing BALB/C mice	Anticancer by combined SDT and IT	119

Note: GSNO: nitrosoglutathione; SNO: *S*-nitrosothiol; L-Arg: L-arginine; SHF: thio-3-hydroxyflavone; MnCO: manganese carbonyl; 3,5-Ph2-tzH: 3,5-diphenyl-1,2,4-triazole.

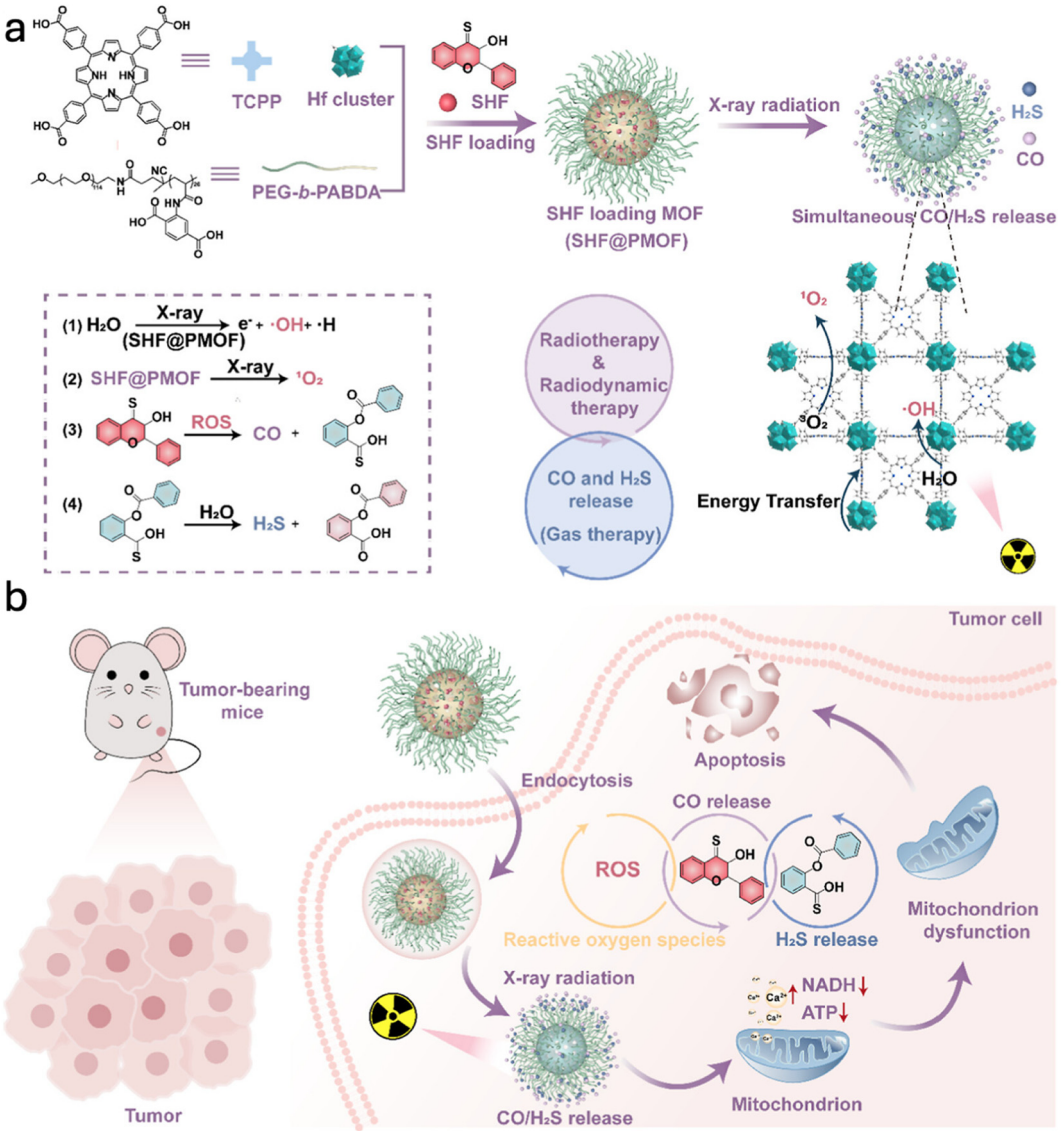

Fig. 4 The preparation and antitumor mechanism of SHF@PMOF under X-ray irradiation. (a) Synthesis of SHF@PMOF and dual release of CO and H_2S triggered by X-ray irradiation, enabling synergistic tumor therapy through RT-RDT and gas therapy. (b) Antitumor efficacy of the combined RT-RDT and gas therapy, where CO/H_2S release induces mitochondrial dysfunction and significantly enhances tumor radiosensitivity. This figure has been reproduced from ref. 109 with permission from American Chemical Society, copyright 2025.

the absence of irradiation, whereas significant cell death was observed only upon X-ray exposure, attributable to the synergistic effects of dual-gas therapy and PMOF-mediated RT-RDT. Beyond gas delivery, MOFs can also act as traceable agents through their intrinsic fluorescence, enabling real-time monitoring of gas release in the tumor microenvironment. For instance, Jin and colleagues[110] reported a Ti-MOF composed of Ti^{4+} and 2,2′-bipyridine-4,4′-dicarboxylic acid (BPYDC), in which the organic ligand BPYDC endowed the framework with inherent fluorescence. Coordination with MnCO quenched this signal, but fluorescence was reactivated during CO release triggered by intracellular H_2O_2, further providing a unique means to monitor CO release within cells. Moreover, with a high loading capacity of 53.2 wt% MnCO, the system remained stable under normal conditions but selectively released CO in response to elevated H_2O_2, enabling tumor-specific delivery. Collectively, these findings demonstrate that MOFs can function as protective carriers for gas donors, preventing premature degradation, while enabling stimulus-responsive gas generation and serving as therapeutic amplifiers to enhance anticancer efficacy.

In contrast, although O_2 and H_2 lack the intrinsic bioactivity characteristic of classical therapeutic gases such as NO, CO, and H_2S, they have been investigated for their auxiliary roles in cancer-related treatment strategies, primarily through modulation or enhancement of complementary therapeutic modalities. Owing to their relatively low toxicity and higher chemical stability, these gases are generally considered safer, and their administration can be achieved *via* direct delivery approaches. In general, O_2 delivery helps alleviate hypoxia in the tumor microenvironment, either through endogenous production or

through exogenous delivery. In the study by Cai and co-workers,[111] a novel Cu–Tz1 system composed of highly active Cu^+ and 3,5-diphenyl-1,2,4-triazole (3,5-Ph2-tzH) was designed to carry O_2 exogenously while simultaneously promoting O_2 generation *via* a Fenton-like reaction. Cu–Tz1 demonstrated a notable O_2 adsorption capacity of up to 400 μmol g^{-1} and, under irradiation, released O_2 at concentrations up to 6 mg L^{-1} within 20 min. This system exhibited superior tumor growth inhibition by effectively combining gas therapy and PDT, as confirmed in 4T1 tumor-bearing mouse models. Meanwhile, investigations into the potential role of H_2 in cancer-related applications remain relatively limited compared with those of other gas molecules. Recent studies have suggested that H_2 may exhibit biological activities, such as antioxidative and cytoprotective effects; however, its underlying mechanisms and therapeutic relevance in oncology are still under active exploration.[112] In this regard, MOF-based platforms have been explored as feasible carriers for the exogenous delivery of H_2. For instance, Zhou and co-workers[113] reported a Pd–MOF system in which Pd^{2+} sites enabled sustained H_2 release for up to 120 h, reaching concentrations of approximately 6 μM. The combined effects of H_2 delivery and the photothermal properties of the Pd–MOF were proposed to contribute to tumor inhibition. While *in vitro* and *in vivo* results indicated that the Pd–MOF system could effectively transport H_2 and enhance photothermal performance, these findings primarily serve as an initial demonstration of feasibility. Further systematic investigations are therefore needed to clarify the mechanistic contributions of H_2 and to assess its long-term therapeutic potential in cancer applications.

7. Applications of MOF-based multi-cargo delivery systems

As previously discussed, anticancer efficacy has been demonstrated for drugs, nucleic acids, proteins, and gases delivered *via* MOF structures, with each type offering distinct advantages and having been extensively studied. Building on this, advanced systems have been developed by combining molecules to create multifunctional therapies that maximize the benefits of each component. MOFs, with the advances from their structural characteristics, are suitable for accommodating and delivering multiple cargoes toward cancer therapy, boosting the antitumor effect. These studies are summarized in Table 5 and will be discussed in the following section.

Drug-based therapies remain central in cancer treatment, but their efficacy can be greatly reinforced when combined with other bioactive molecules. However, the co-loading of small molecules (*e.g.*, drugs) and macromolecules (*e.g.*, nucleic acids and proteins) remains challenging due to their distinct structural characteristics and intrinsic instability. In this context, several MOF platforms exploited their porous structure, with a certain type offering large internal voids and unsaturated coordination sites to promote strong interactions with multiple bioactive molecules, thereby enabling high loading efficiency and enhanced protection of encapsulated cargos against premature degradation. A representative example of drug–nucleic acid combination therapy is provided by the study of Chen and colleagues.[120] They developed MOF-801, a Zr^{4+}–fumaric acid framework capable of co-loading CpG-ODN (8.3 wt%) and dimethylxanthenone acetic acid (DMXAA) (1.5 wt%) (Fig. 5). The MOF-801 platform was shown to exhibit ATP-responsive behavior and was hypothesized to function as a STING agonist, thereby activating the cGAS–STING–NF-κB pathway to enhance innate anticancer immunity. Compared with free CpG-ODN or DMXAA, which induced low levels of inflammatory cytokines, particularly IL-6 and TNF-α, MOF-CpG-ODN and MOF-DMXAA elicited significantly higher cytokine expression. Notably, the co-loaded MOF-CpG-DMXAA formulation produced the highest levels of inflammatory mediators among all groups, highlighting a clear enhancement relative to single-agent treatments. These strategies have been widely reported in recent studies, with the preferences in employing stable and biocompatible MOFs such as ZIF-8 and Zr-MOF, whose primary advantage is providing a safe and protective shell for fragile structures like nucleic acids.[121–124] A similar trend was observed in drug–protein co-delivery. In a study by Dai *et al.*,[125] Mn^{2+} and the ROS-susceptible linker 5,5-dimethyl-4,6-dithia-nonanedioic acid (DTA) were used to construct Mn-DTA, allowing post-loading of 1-methyltryptophan (1-MT) at 13.5 wt% and GOx at 8.8 wt%. Owing to its low bioavailability, 1-MT typically requires repeated administration at high doses to achieve therapeutic efficacy. In this context, PCP-Mn-DTA@GOx@1-MT markedly prolonged the circulation time of 1-MT and enhanced its tumor accumulation, resulting in an approximately 5-fold increase compared with free 1-MT. By integrating the complementary therapeutic effects of GOx and 1-MT, the PCP-Mn-DTA@GOx@1-MT formulation achieved the highest tumor inhibition rate among all treatment groups. Additionally, other macromolecules, such as cholesterol oxidase (COD), can be effectively loaded onto the MOF structures. As reported by Guo and colleagues,[98] ZrMOF(Cu) was synthesized successfully at the nanoscale, which has a mesoporous structure with a pore size of 5.99 nm, offering advances for the adsorption of COD and DOX onto the system.

The combination of two types of small molecules of drug–gas is also a potential direction. Du and colleagues[32] employed a highly porous Cu-BTC structure to co-deliver the immunosuppressive enzyme inhibitor BMS-986205 and the NO donor SNAP (Fig. 6). Cu-BTC exhibited an impressive surface area of 1161.75 m^2 g^{-1} and a pore size of 2.02 nm, achieving loading capacity values of 52.5% for BMS-986205 and 62.0% for SNAP. Under elevated GSH levels, Cu^{2+} was reduced to highly active Cu^+, which not only controlled cargo release but also facilitated SNAP-mediated NO generation. The combined gas therapy and enzyme inhibition markedly reduced tumor volumes compared to single-agent MOFs. Within this concept, Yang *et al.*[126] designed a dual-responsive MOF-5 system sensitive to both pH and GSH for the co-delivery of dihydroartemisinin (DHA) and carbon monoxide-releasing molecule 401 (CORM-401). Both cargos were effectively co-loaded into MOF-5 with impressive loading capacity values of 21.1 wt% for DHA and 16.7 wt% for CORM-401. Under the trigger of pH and GSH, the delivery system revealed the effective release of

Table 5 Applications of MOF-based multi-cargo delivery systems for cancer therapy

Delivery system	Cargo	MOF components	Stimuli	*In vitro*	*In vivo*	Application	Ref.
MOF-CpG-DMXAA	DMXAA (drug); CpG (nucleic acid)	Zr^{4+}, fumaric acid	ATP	Hepa1-6	Hepa1-6 tumor-bearing C57BL/6 mice	Anticancer by IT	120
ALA&Dz@ZIF-PEG	ALA (drug); DNAzyme (nucleic acid)	Zn^{2+}, 2-MIM	pH, visible laser irradiation	MCF-7, 4T1, CT26	MC7 and 4T1 tumor-bearing BALB/C nude mice	Anticancer by combined PDT and IT	123
TPL/siHIF-1α@Zr-MOF@CM	TPL (drug); siHIF-1α (nucleic acid)	Zr^{4+}, TCPP	pH, visible laser irradiation	Kyse-30	Kyse-30 tumor-bearing BALB/C nude mice	Anticancer by combined gene therapy and PDT	122
Aptamer/(siRNA + GEF)@ZIF-8	GEF (drug); siRNA (nucleic acid)	Zn^{2+}, 2-MIM	pH	PC-9, A549	PC-9 tumor-bearing BALB/C nude mice	Anticancer effect by gene therapy	121
PCN-ACF-CpG@HA	ACF (drug); CpG (nucleic acid)	Zr^{4+}, TCPP	Intratumoral HAase, visible laser irradiation	H22	H22 tumor-bearing BALB/C mice	Anticancer by combined PDT and IT	124
MCM@PEG-CO-DOX	DOX (drug); MnCO (gas)	Fe^{3+}, BTC	NIR irradiation	HCT116	HCT116 tumor-bearing BALB/C nude mice	Anticancer by combined gas therapy, CT and PTT	116
BMS-SNAP-MOF	BMS (drug); SNAP (gas donor)	Cu^{2+}, BTC	GSH	4T1	4T1 tumor-bearing BALB/C mice	Anticancer by combined gas therapy and IT	32
ICG-PFH/MOF/DNA-DOX	DOX (drug); PFH (gas)	Zr^{4+}, BDC-N_3	pH, NIR laser irradiation, ATP	HepG2, 4T1	HepG2 tumor-bearing BALB/C nude mice	Anticancer by combined PTT, PDT and CT	128
pHCT74/MOF-5@DHA&-CORM-401	DHA (drug); CORM-401 (gas)	Zn^{2+}, BDC	pH, GSH	CT26	CT26 tumor-bearing BALB/C mice	Anticancer by combined gas therapy, CT and IT	126
(DOX@AFt + GOx)@ZIF-8 corona bioMOF	DOX (drug); AFt (protein); GOx (protein)	Zn^{2+}, 2-MIM	pH	MX-1, MDA-MB-231	MDA-MB-231 tumor-bearing BALB/C nude mice	Anticancer by targeted delivery and enhanced CT	129
PCP-Mn-DTA@GOx@1-MT	1-MT (drug); GOx (protein)	Mn^{2+}, DTA	pH, intracellular ROS	B16F10	B16F10 and 4T1 tumor-bearing C57BL/6 mice and BALB/C mice	Anticancer by combined IT, CDT and cancer starvation therapy	125
CUR/GOx@LCOF	CUR (drug); GOx (protein)	Cu^{2+}, BTC	pH	4T1	4T1 tumor-bearing BALB/C mice	Anticancer by combined CT, CDT and cancer starvation therapy	130
DOX@COD-MOF@CCM	DOX (drug); COD (protein)	Zr^{4+}, Cu^{2+}, BPYDC	pH	MCF-7/ADR, MCF-7, HepG2, 4T1	MCF-7/ADR tumor-bearing BALB/C nude mice	Anticancer by CT and enhanced apoptosis	98
Fe-DNA/GOx@ZIF-8	DNA (nucleic acid); GOx (protein)	Zn^{2+}, 2-MIM	pH	4T1, HeLa	4T1 tumor-bearing BALB/C mice	Anticancer by combined CDT and cancer starvation therapy	127
MnCO@UiO-67-bpy@GOx (CORM@GOx)	MnCO (gas); GOx (protein)	Zr^{4+}, BPYDC	Intracellular H_2O_2	HeLa, MCF-7	HeLa tumor-bearing nude mice	Anticancer by combined gas therapy and CDT	118

Note: CpG: CpG oligodeoxynucleotides; DMXAA: dimethylxanthenone acetic acid; ALA: 5-aminolevulinic acid; TPL: triptolide; siHIF-1α: small interfering RNA (siRNA) targeting the hypoxia-inducible factor 1 alpha (HIF-1α) gene; GEF: gefitinib; ACF: acriflavine; BMS: immunosuppressive enzyme indoleamine 2,3-dioxygenase inhibitor BMS-986205; SNAP: *S*-nitroso-*N*-acetylpenicillamine; PFH: perfluorohexane; DHA: dihydroartemisinin; AFt: apoferritin; 1-MT: 1-methyltryptophan; HAase: hyaluronidase; CORM: carbon monoxide-releasing molecule.

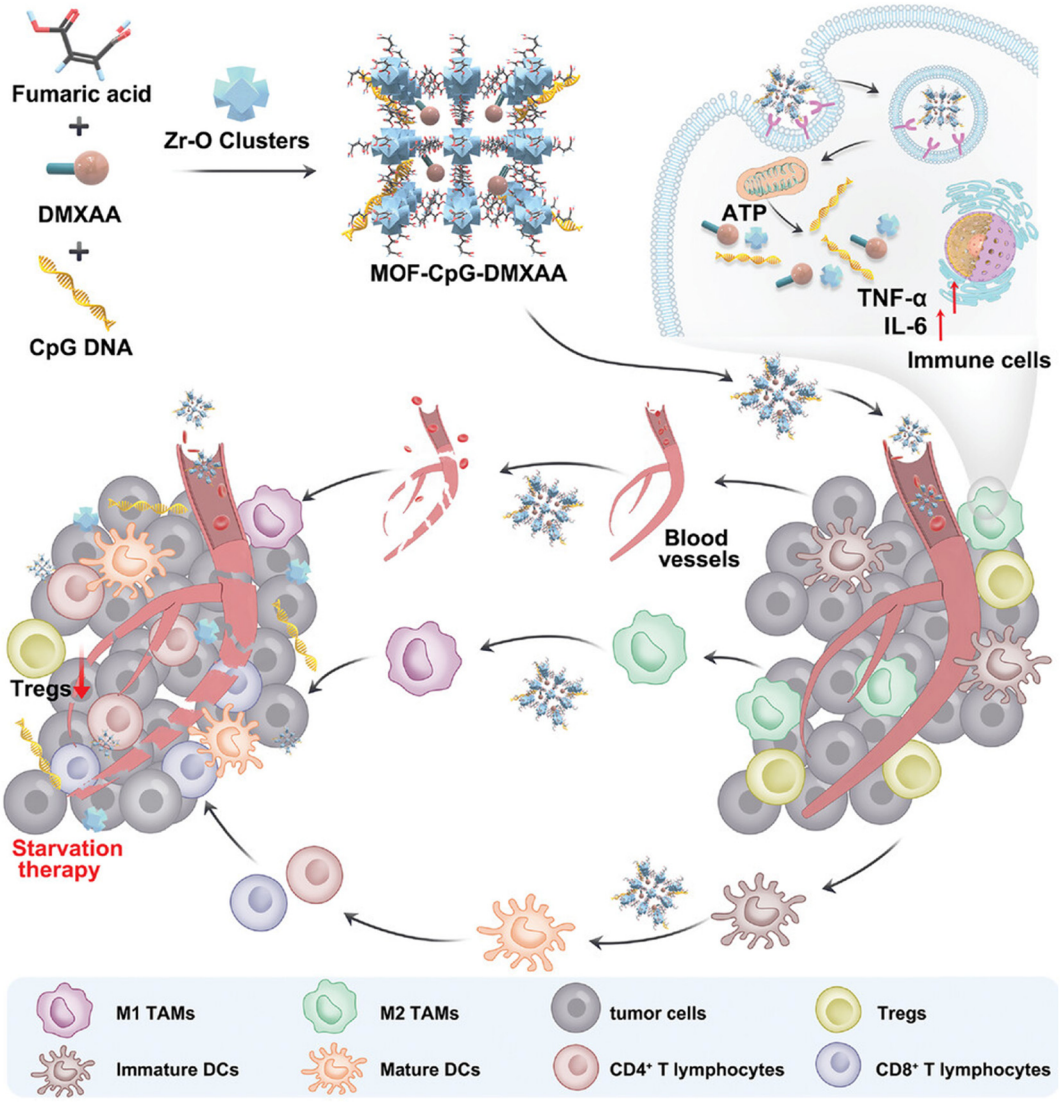

Fig. 5 Schematic representation of the synthesis and immunotherapeutic mechanism of MOF-CpG-DMXAA. CpG ODNs and the vascular-disrupting agent DMXAA are co-encapsulated within MOF-801. While each component activates the cGAS–STING–NF-κB signaling pathway to reprogram tumor-associated macrophages (TAMs) and promote dendritic cell (DC) maturation, the integrated MOF-CpG-DMXAA system elicits systemic immune activation and tumor vascular disruption, resulting in superior efficacy of IT. This figure has been reproduced from ref. 120 with permission from John Wiley and Sons, copyright 2023.

DHA and CORM-401 of more than 80% after 50 h. Beyond cargo encapsulation, MOF-5 also consumed intracellular GSH, thereby amplifying the therapeutic performance of the active agents. Besides these strategies, other combinations (*e.g.*, nucleic acid–protein, gas–protein) have also been presented in many recent studies with proven effectiveness toward cancer therapy, aiming to maximize antitumor effects by exploiting the abnormal conditions of the tumor microenvironment, thereby offering multifunctional advanced MOF-based systems to overcome limitations.[118,127]

8. Limitations and future prospects

Although MOF-based delivery systems show significant potential in transporting drugs, nucleic acids, proteins, and therapeutic gases, their translation from laboratory studies to clinical applications remains limited. This limitation is caused by their intrinsic chemical and physical properties. It is also influenced by the complexity of the tumor microenvironment. Difficulties in large-scale production and strict safety requirements further limit their progress toward clinical use.

8.1. Limitations

(i) The structural versatility of MOFs enables their responsiveness to multiple stimuli. However, this flexibility may also introduce stability-related trade-offs. From a manufacturing perspective, precise control of synthesis and storage conditions is required to maintain structural integrity and functional performance. This increases production complexity and may affect therapeutic consistency. In biological environments, certain MOFs are susceptible to premature degradation. The metal centers are often kinetically labile and can be displaced by endogenous proteins (*e.g.*, albumin) and competing anions (*e.g.*, phosphate-based ions).[131] This

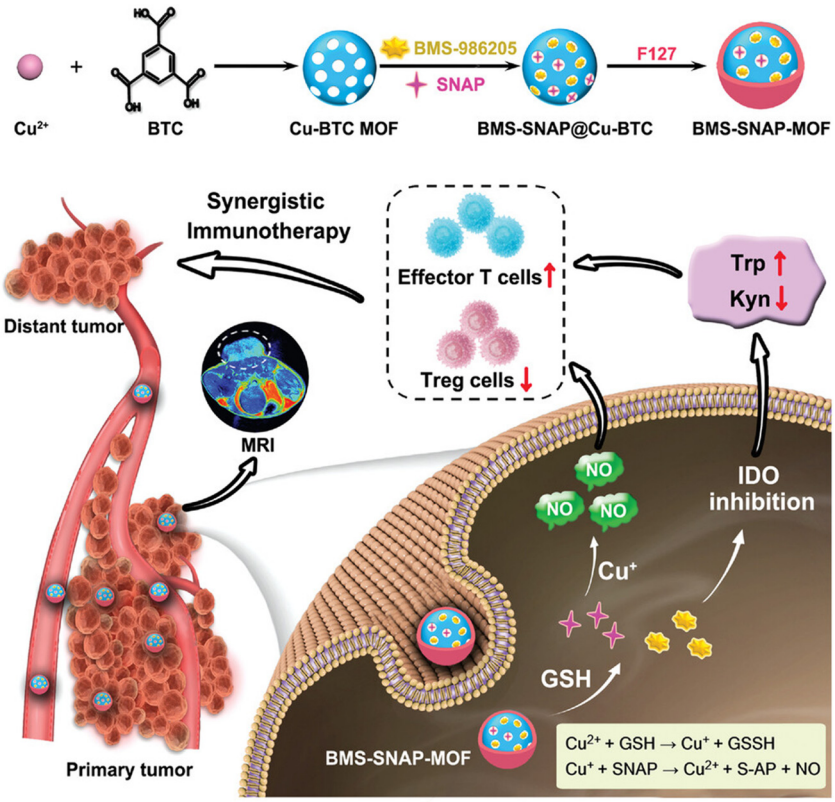

Fig. 6 Schematic illustration of the synthesis and synergistic immunotherapeutic mechanism of BMS-SNAP-MOF. Under GSH stimulation, the system releases Cu^{2+}, which is reduced to Cu^{+} and reacts with SNAP to generate NO, thereby amplifying the antitumor efficacy of IT. This figure has been reproduced from ref. 32 with permission from John Wiley and Sons, copyright 2022.

limitation is particularly relevant because physiological environments are far more complex and heterogeneous than simplified *in vitro* models. The tumor microenvironment, in particular, involves multiple dynamic and overlapping biological factors beyond well-recognized stimuli, which may influence MOF stability and behavior.

(ii) Metal ions commonly incorporated into MOF structures play essential physiological roles when tightly regulated under homeostatic conditions; however, excessive accumulation of these ions may lead to biological dysregulation. This raises important concerns regarding the long-term toxicity and *in vivo* fate of metal species released from MOFs. The biocompatibility of MOFs remains under ongoing discussion. Although biodistribution analyses and preliminary histological evaluations often indicate minimal acute toxicity, several critical aspects remain insufficiently characterized. These include tolerated accumulation thresholds, long-term biological effects, and the impact of degradation products. Such knowledge gaps continue to limit comprehensive safety evaluation and translational assessment.

(iii) Optimized MOF synthesis protocols often require considerable time to achieve materials with controlled size, morphology, and crystallinity. However, it cannot be fully guaranteed that protocols optimized at the laboratory scale will maintain consistent batch-to-batch productivity upon scale-up. Reproducibility, therefore, represents a primary challenge for large-scale production. Moreover, priorities at the laboratory scale differ fundamentally from those at the industrial level. Laboratory research typically emphasizes structural optimization, with reaction conditions tailored to achieve precise control over size, morphology, and crystallinity. In contrast, large-scale production must ensure high yield, process robustness, cost-effectiveness, and minimal environmental impact. Many MOFs require stringent control of synthesis parameters, including highly purified precursors, elevated temperatures or pressures, and the use of toxic or volatile solvents (*e.g.*, DMF). These requirements increase energy consumption and production costs, thereby raising economic, environmental, and safety concerns. Collectively, these constraints pose significant challenges to the scalable and cost-effective industrial translation of MOF synthesis.

(iv) Advanced MOF-based strategies have demonstrated promising efficacy in both *in vitro* and *in vivo* studies. However, translation to the clinical stage remains challenging. According to statistics, despite favorable outcomes in animal models, approximately 86% of investigational therapeutics fail in clinical trials.[132] In the case of MOFs, although more than 90 000 MOF structures have been reported, only a few platforms have progressed to initial phases of clinical evaluation.[131] This gap highlights the translational barriers facing MOF-based biomedical applications and underscores the need for more predictive and clinically relevant evaluation models to improve clinical translation.

(v) Recent advances in the design of multi-cargo MOF systems are primarily driven by the ambition to simultaneously

address multiple therapeutic objectives in cancer treatment. While conceptually attractive, such multifunctional platforms inevitably introduce experimental complexity with prolonged development timelines. Despite encouraging preliminary results, these systems have not yet been rigorously benchmarked against FDA-approved therapies with well-validated clinical efficacy.[133] This raises important questions regarding the urgency and practical necessity of developing increasingly complex material systems. Whether MOF-based platforms can ultimately achieve comparable or superior clinical benefit therefore remains uncertain and warrants rigorous validation to substantiate their translational relevance.

8.2. Future prospects

(i) One future direction is the development of more biocompatible MOFs by the alternation of the two fundamental components used to construct MOFs. The use of endogenous or less toxic ions such as Ca^{2+}, Mg^{2+}, Zn^{2+}, or Fe^{3+} can reduce long-term toxicity. In parallel, the incorporation of bio-derived ligands represents a promising strategy to further enhance the safety profile, biocompatibility, and clinical adaptability of MOF-based systems. However, due to differences in coordination behavior and structural properties compared to conventional linkers, bio-derived ligands may alter framework formation, crystallinity, and stability. Therefore, comprehensive structural and physicochemical evaluations are essential when implementing such modifications.

(ii) The toxicological assessment of metal ions and MOF degradation products requires more rigorous and physiologically relevant investigation. Current evaluations are often limited to simplified environments, such as buffered aqueous solutions or cell culture media. Future studies should extend to serum-containing systems and conditions that more accurately mimic physiological pH and enzymatic activity. Moreover, preclinical animal studies have predominantly been conducted in murine models, rabbits, or zebrafish, with primary emphasis on acute biocompatibility, systemic toxicity, organ function, and histopathology following single-dose administration. Comprehensive long-term and multi-dose studies are critically needed to elucidate potential cumulative and chronic effects associated with MOF exposure.

(iii) Advanced evaluation models should also be incorporated into the research scope of MOF-based cancer therapies. Emerging platforms such as organoids and organ-on-a-chip technologies can closely simulate tumor microenvironment dynamics and provide more physiologically relevant testing platforms. Validation using these advanced models represents a crucial intermediate step toward strengthening the translational foundation required for progression into clinical phases.

(iv) Artificial intelligence (AI) and computational modeling hold significant promise in accelerating MOF design and optimization. AI-driven approaches can predict metal–ligand coordination behavior, optimize pore architectures, simulate cargo loading and release kinetics, forecast potential toxicity, and identify rational multi-cargo combinations. Such *in silico* strategies align with global scientific and technological trends while substantially reducing experimental time.

(v) The further development of green and mild synthetic strategies should be prioritized to facilitate the transition toward large-scale production. In parallel, comprehensive standardization of methodologies and evaluation guidelines is essential to enhance data validity and improve inter-laboratory reproducibility. Together, these efforts will facilitate a more rigorous, efficient, and practically relevant evaluation of the technological and pharmaceutical potential of MOF-based systems.

9. Conclusion

In this review, we have summarized recent advances in the development and application of MOF-based systems as versatile delivery platforms for cancer therapy. By highlighting their structural advantages and multifunctional capabilities, we show how MOFs can efficiently encapsulate and deliver diverse therapeutic cargos, enabling controlled release and enhanced treatment performance. These findings underscore the adaptability of MOFs and their strong potential to support next-generation cancer therapeutics. Despite significant progress, this field remains in its early stages and continues to offer substantial opportunities for further advancement. Critical challenges associated with the translation of MOF-based drug delivery systems for cancer therapy, particularly those related to scalable manufacturing and clinical implementation, require rigorous and systematic investigation. Overcoming these barriers is key to unlocking the potential of MOF platforms for precise and effective cancer treatment. We hope that the insights provided in this review will contribute a more comprehensive perspective of MOF-based systems, inspire future research, and accelerate the advancement of innovative MOF-based therapeutic strategies.

Author contributions

Luan Minh Nguyen: conceptualization, investigation, supervision, project administration, writing – original draft, writing – review & editing. Giao Thuy Quynh Vu: investigation, visualization, methodology, formal analysis, writing – original draft. Ngoan Thi Thao Nguyen: methodology, writing – original draft. Thuy Thi Thanh Nguyen: investigation, writing – review & editing. Duyen Thi Cam Nguyen: formal analysis, writing – review & editing. Thuan Van Tran: investigation, writing – review & editing. Ngoc Hoi Nguyen: methodology, investigation. Dai Hai Nguyen: supervision, validation, funding acquisition, project administration. All authors read and approved the final manuscript.

Conflicts of interest

The authors declare that they have no known competing financial interests or personal relationships that could have appeared to influence the work reported in this paper.

Data availability

Data will be made available on request.

Acknowledgements

This work was supported by the Vietnam Academy of Science and Technology (VAST) under the project number NCXS01.01/24-26.

References

1 Y. Gu, R. Yang, Y. Zhang, M. Guo, K. Takehiro, M. Zhan, L. Yang and H. Wang, *Mol. Biomed.*, 2025, **6**, 2.
2 X. Xiong, L.-W. Zheng, Y. Ding, Y.-F. Chen, Y.-W. Cai, L.-P. Wang, L. Huang, C.-C. Liu, Z.-M. Shao and K.-D. Yu, *Signal Transduction Targeted Ther.*, 2025, **10**, 49.
3 K. Li, B. Guo, J. Gu, N. Ta, J. Gu, H. Yu, M. Sun and T. Han, *Mater. Today Bio*, 2025, **30**, 101375.
4 Y. Miao, Z. Wang, F. Song, R. Gao, Z. Deng and G. Zhang, *Adv. Funct. Mater.*, 2025, **35**, 2510183.
5 N. Nasri, M. Azad, Z. Mehrabi, G. Dini and A. Marandi, *RSC Adv.*, 2025, **15**, 34481–34509.
6 H. Furukawa, K. E. Cordova, M. O'Keeffe and O. M. Yaghi, *Science*, 2013, **341**, 1230444.
7 L. M. Nguyen, N. T. T. Nguyen, T. T. T. Nguyen, D. H. Nguyen, D. T. C. Nguyen and T. Van Tran, *Environ. Res.*, 2022, **215**, 114269.
8 P. Das, G. Chakraborty, J. Kaur and S. K. Mandal, *Small*, 2025, **21**, 2408810.
9 S. Feng, Y. Li, Z. Tan and S. Shen, *Int. J. Pharm.*, 2025, **672**, 125295.
10 L. M. Nguyen, G. T. Q. Vu, N. T. T. Le, T. P. Nguyen, T. Nguyen-Dinh, D. L. Tran, L. B. Vong and D. H. Nguyen, *Surf. Interfaces*, 2026, **80**, 108246.
11 M. T. Khulood, U. S. Jijith, P. P. Naseef, S. M. Kallungal, V. S. Geetha and K. Pramod, *Int. J. Pharm.*, 2025, **673**, 125380.
12 L. M. Nguyen, Y. Wang, G. T. Quynh Vu, Q. T. Hoai Ta, D. L. Tran, N. H. Nguyen, T. Van Tran, C. Zhang and D. H. Nguyen, *Nanoscale Adv.*, 2025, **7**, 5479–5500.
13 C. Zhao, W. Song, J. Wang, X. Tang and Z. Jiang, *Chem. Commun.*, 2025, **61**, 1962–1977.
14 M. Cai, Y. Yang, J. Kong, Y. Zhang, S. Li, H. Zhang, X. Xv, J. Ni and X. Yin, *J. Nanobiotechnol.*, 2025, **23**, 601.
15 P. Gong, F. Wang, Y. Hua, J. Ying, J. Chen and Y. Qiao, *J. Nanobiotechnol.*, 2025, **23**, 733.
16 M. Demicco, X.-Z. Liu, K. Leithner and S.-M. Fendt, *Nat. Metab.*, 2024, **6**, 18–38.
17 X. Jing, H. Hu, Y. Sun, B. Yu, H. Cong and Y. Shen, *Small Methods*, 2022, **6**, 2101437.
18 T. L. Nguyen, Y. Choi and J. Kim, *Adv. Mater.*, 2019, **31**, 1803953.
19 S. Priya, V. M. Desai and G. Singhvi, *ACS Omega*, 2023, **8**, 74–86.
20 M. A. Beach, U. Nayanathara, Y. Gao, C. Zhang, Y. Xiong, Y. Wang and G. K. Such, *Chem. Rev.*, 2024, **124**, 5505–5616.
21 Y. Chao and Z. Liu, *Nat. Rev. Bioeng.*, 2023, **1**, 125–138.
22 G. T.-Q. Vu, L. M. Nguyen, K. N. Nguyen Do, D. L. Tran, T. Van Vo, D. H. Nguyen and L. B. Vong, *ACS Appl. Bio Mater.*, 2025, **8**, 2052–2064.
23 K. Zheng, Y. Shen, J. Li, H. Zhang, Y. Dong and J. Li, *Colloids Surf., A*, 2026, **730**, 139006.
24 T. Xue, C. Xu, Y. Wang, Y. Wang, H. Tian and Y. Zhang, *Biomater. Sci.*, 2019, **7**, 4615–4623.
25 N. Yang, W. Xiao, X. Song, W. Wang and X. Dong, *Nano-Micro Lett.*, 2020, **12**, 15.
26 G. Cognet and A. Muir, *Sci. Adv.*, 2024, **10**, eadq7305.
27 S. Zhou, F. Jia, Y. Wei, J. Du, J. Liu, W. Dong, J. Sui, W. Xue, Y. Yang, L. Chen, X. Meng and S. Yu, *Adv. Funct. Mater.*, 2024, **34**, 2314012.
28 C. Huang, W. Tan, J. Zheng, C. Zhu, J. Huo and R. Yang, *ACS Appl. Mater. Interfaces*, 2019, **11**, 25740–25749.
29 K. Zhang, X. Meng, Z. Yang, H. Dong and X. Zhang, *Biomaterials*, 2020, **258**, 120278.
30 G. Vilema-Enríquez, A. Arroyo, M. Grijalva, R. I. Amador-Zafra and J. Camacho, *Oxid. Med. Cell. Longevity*, 2016, **2016**, 1908164.
31 Y. Ding, Y. Dai, M. Wu and L. Li, *Chem. Eng. J.*, 2021, **426**, 128880.
32 L. Du, H. He, Z. Xiao, H. Xiao, Y. An, H. Zhong, M. Lin, X. Meng, S. Han and X. Shuai, *Small*, 2022, **18**, 2107732.
33 S. Chatterjee, A. Rai, R. Patwardhan, R. Agrawal, P. Chandwadkar, D. Pal, S. Gorai, C. Acharya, A. D. Ballal, S. K. Sandur and D. Goswami, *ACS Appl. Nano Mater.*, 2024, **7**, 8197–8211.
34 H. Yao, R. Ji, X. Song, B. Yang, Y. Lv and Z. Wei, *New J. Chem.*, 2025, **49**, 11423–11433.
35 Y. Li, X. Zhang, J. Wang, K. Wang, B. Li, X. Qiao, W. He, J. Cai, D. Liu and L.-L. Yang, *Theranostics*, 2025, **15**, 4708–4733.
36 F. Di Virgilio, A. C. Sarti, S. Falzoni, E. De Marchi and E. Adinolfi, *Nat. Rev. Cancer*, 2018, **18**, 601–618.
37 H. Jin, H. Yang, W. Huang, N. Zhong, Y. Xu, A. Huang, X. Liu, S. Huang, F. Zhu, G. Chen and G. Ouyang, *Anal. Chem.*, 2025, **97**, 19982–19991.
38 X.-F. Xu, J.-T. Chen, Q. Song, Z.-Q. Wang, J.-Q. Long, G.-J. Mao, Y. Li, L. Hu, J. Ouyang and C.-Y. Li, *Nanoscale*, 2025, **17**, 15804–15814.
39 Z. Guo, Y. Xiao, W. Wu, M. Zhe, P. Yu, S. Shakya, Z. Li and F. Xing, *J. Nanobiotechnol.*, 2025, **23**, 157.
40 F. Xing, J. Xu, Y. Zhou, P. Yu, M. Zhe, Z. Xiang, X. Duan and U. Ritz, *Nanoscale*, 2024, **16**, 4434–4483.
41 X. Du, R. Fan, L. Qiang, K. Xing, H. Ye, X. Ran, Y. Song, P. Wang and Y. Yang, *ACS Appl. Mater. Interfaces*, 2017, **9**, 28939–28948.
42 Y. Miao, W. Pan, K. Chen, H. Wei, F. Mi, M. Lu, Y. Chang and H. Sung, *Adv. Funct. Mater.*, 2019, **29**, 1904828.
43 S. Iqbal, T.-J. K. Schneider, T. T. Truong, R. Ulrich-Müller, P.-H. Nguyen, S. Ilyas and S. Mathur, *Nanoscale*, 2024, **16**, 11274–11289.
44 L. M. Nguyen, G. T. Q. Vu, M. H. Tran, T. M. H. Nguyen, T. P. Nguyen, D. L. Tran, L. B. Vong and D. H. Nguyen, *Inorg. Chem. Commun.*, 2026, **183**, 115867.
45 Y. Mirchandani, V. B. Patravale and S. Brijesh, *J. Controlled Release*, 2021, **335**, 457–464.
46 M. Xu, H. Chen, G. Zhu, X. Zhu, R. Gao, B. Xu, X. Song, X. Han, T. Shao, Q. Sun, Z. Xiao, H. Wang, Y. Zhang, G. Yang and J. Li, *Nano Today*, 2024, **56**, 102231.

47 X. Wang, X. Lu, X. Yang, B. Zhu, W. Deng, Q. Ye, B. Bai, D. Liang, B. Shao, Y. Huang, T. You, W. Zhang, W. Sun and X. Shen, *Mater. Des.*, 2024, **238**, 112731.
48 G. Tan, Y. Zhong, L. Yang, Y. Jiang, J. Liu and F. Ren, *Chem. Eng. J.*, 2020, **390**, 124446.
49 L. M. Nguyen, G. T. Q. Vu, M. H. Tran, T. M. H. Nguyen, T. P. Nguyen, Q. T. H. Ta, D. L. Tran and D. H. Nguyen, *Mater. Adv.*, 2025, **6**, 7574–7584.
50 M. Babaei, A. Abrishami, S. Iranpour, A. S. Saljooghi and M. M. Matin, *Drug Delivery Transl. Res.*, 2025, **15**, 1719–1738.
51 S. Yang, Z. Zhao, Y. Xie, J. Lin, B. Zhang and J. Fan, *Int. J. Pharm.*, 2022, **623**, 121912.
52 L. M. Nguyen, G. T.-Q. Vu, T.-K.-C. Huynh, Q. T. H. Ta, N. H. Nguyen, D. L. Tran and D. H. Nguyen, *Colloids Surf., A*, 2025, **711**, 136321.
53 Q. Zhang, G. Kuang, H. Wang, Y. Zhao, J. Wei and L. Shang, *Adv. Sci.*, 2023, **10**, 2303818.
54 B. Li, X. Yao, J. Li, X. Lu, W. Zhang, W. Duan, Y. Tian and D. Li, *J. Biol. Chem.*, 2023, **299**, 102742.
55 S. Gao, Y. Jin, K. Ge, Z. Li, H. Liu, X. Dai, Y. Zhang, S. Chen, X. Liang and J. Zhang, *Adv. Sci.*, 2019, **6**, 1902137.
56 M. Zhang, X. Yao, J. Xu, J. Song, S. Mai, W. Zhu, Y. Zhang, L. Zhu and W. Yang, *Int. J. Pharm.*, 2024, **655**, 124032.
57 Z. Li, Y. Liu, K. Zhou, L. Cao, G. Wang, J. Wu, Y. Yu, Y. Xiao, B. Liu, Q. Wu, Z. Song and L. Bu, *Adv. Sci.*, 2025, **12**, e02154.
58 A. Hashemi, S. R. Hayat-Gheibi and F. Baghbani-Arani, *J. Drug Delivery Sci. Technol.*, 2024, **95**, 105515.
59 L. Hu, C. Xiong, G. Wei, Y. Yu, S. Li, X. Xiong, J.-J. Zou and J. Tian, *J. Colloid Interface Sci.*, 2022, **608**, 1882–1893.
60 Y.-X. Ge, T.-W. Zhang, L. Zhou, W. Ding, H.-F. Liang, Z.-C. Hu, Q. Chen, J. Dong, F.-F. Xue, X.-F. Yin and L.-B. Jiang, *Biomaterials*, 2022, **282**, 121407.
61 A. Ehsani, M. Fathi, H. Goshtasbi, H. Erfan-Niya and H. Aghdasinia, *Int. J. Biol. Macromol.*, 2025, **321**, 146459.
62 Y. Li, H. Sun, C. Yang, Z. Yan, J.-Y. Ge, J. Wang, Z. Chen, L. Qiu and Y. Bai, *ACS Appl. Nano Mater.*, 2024, **7**, 10532–10542.
63 W. Ni, L. Zhang, H. Zhang, C. Zhang, K. Jiang and X. Cao, *Inorg. Chem.*, 2022, **61**, 3281–3287.
64 B. Liu, Z. Liu, X. Lu, P. Wu, Z. Sun, H. Chu and H. Peng, *Mater. Des.*, 2023, **228**, 111861.
65 X. Sun, G. He, C. Xiong, C. Wang, X. Lian, L. Hu, Z. Li, S. J. Dalgarno, Y.-W. Yang and J. Tian, *ACS Appl. Mater. Interfaces*, 2021, **13**, 3679–3693.
66 B. Liu, H. Zhou, L. Tan, K. T. H. Siu and X.-Y. Guan, *Signal Transduction Targeted Ther.*, 2024, **9**, 175.
67 T. Travieso, J. Li, S. Mahesh, J. D. F. R. E. Mello and M. Blasi, *npj Vaccines*, 2022, **7**, 75.
68 G. Geng, Y. Xu, Z. Hu, H. Wang, X. Chen, W. Yuan and Y. Shu, *EBioMedicine*, 2025, **118**, 105834.
69 A. Poddar, S. Pyreddy, S. A. Polash, C. M. Doherty and R. Shukla, *Biomater. Biosyst.*, 2022, **8**, 100065.
70 S. A. Polash, A. Poddar, S. Pyreddy, F. Carraro, A. M. D'Angelo, G. Bryant, P. Falcaro and R. Shukla, *ACS Appl. Mater. Interfaces*, 2025, **17**, 3002–3012.
71 H. D. Lawson, H. H. Nguyen, K. Lee, N. Wongsuwan, A. Tupe, M. Lu, M. L. Arral, A. Behre, Z. Ling, K. A. Whitehead, A. W. Feinberg, X. Ren and S. Zheng, *Adv. Funct. Mater.*, 2025, **35**, 2504465.
72 S. A. Polash, G. Bryant, V. Bansal and R. Shukla, *Adv. Mater. Interfaces*, 2025, **12**, e00432.
73 H. Wang, Y. Chen, H. Wang, X. Liu, X. Zhou and F. Wang, *Angew. Chem.*, 2019, **131**, 7458–7462.
74 Z. Yang, R. Qin, D. Ruan, C. Hu, W. Li, J. Zhou, F. Zhang, B. Guo, L. Huang, D. Jaque, Y. Shen and F. Wang, *ACS Nano*, 2025, **19**, 27873–27889.
75 R. Jiang, L. Li and M. Li, *ACS Nano*, 2023, **17**, 22129–22144.
76 N. Sun, Q. Lei, M. Wu, S. Gao, Z. Yang, X. Lv, R. Wei, F. Yan and L. Cai, *Mater. Today Bio*, 2024, **26**, 101053.
77 Y. Zhang, L. Yang, H. Wang, J. Huang, Y. Lin, S. Chen, X. Guan, M. Yi, S. Li and L. Zhang, *Chem. Eng. J.*, 2021, **426**, 131926.
78 M. H. Teplensky, M. Fantham, C. Poudel, C. Hockings, M. Lu, A. Guna, M. Aragones-Anglada, P. Z. Moghadam, P. Li, O. K. Farha, S. Bernaldo de Quirós Fernández, F. M. Richards, D. I. Jodrell, G. Kaminski Schierle, C. F. Kaminski and D. Fairen-Jimenez, *Chem*, 2019, **5**, 2926–2941.
79 Y. Qian, Z. Han, D. Yang, Y. Cai, J. Jin and Z. Yang, *Langmuir*, 2023, **39**, 8205–8214.
80 Z. Wang, J. Niu, C. Zhao, X. Wang, J. Ren and X. Qu, *Angew. Chem.*, 2021, **133**, 12539–12545.
81 S. Huang, W. Zhu, F. Zhang, G. Chen, X. Kou, X. Yang, G. Ouyang and J. Shen, *ACS Appl. Mater. Interfaces*, 2021, **13**, 56972–56987.
82 C. Li, D. Yi, M. Li and Z. Li, *Nano Today*, 2025, **65**, 102837.
83 N. Mokri, Z. Sepehri, F. Faninam, S. Khaleghi, N. M. Kazemi and M. Hashemi, *Gene Ther.*, 2022, **29**, 680–690.
84 T. Tripathi, V. N. Uversky and A. Giuliani, *Cell. Mol. Life Sci.*, 2025, **82**, 239.
85 Y. Guo, Y. Li, S. Zhou, Q. Ye, X. Zan and Y. He, *ACS Biomater. Sci. Eng.*, 2022, **8**, 4028–4038.
86 M. Kai, S. Wang, W. Gao and L. Zhang, *J. Controlled Release*, 2023, **361**, 178–190.
87 S. B. Ebrahimi and D. Samanta, *Nat. Commun.*, 2023, **14**, 2411.
88 C. Wang, J. Yang, C. Dong and S. Shi, *Adv. Ther.*, 2020, **3**, 2000110.
89 L. Shao, X. Gao, J. Liu, Q. Zheng, Y. Li, P. Yu, M. Wang and L. Mao, *ACS Appl. Mater. Interfaces*, 2022, **14**, 47472–47481.
90 J. Zhou, K. Wang, S. Ding, L. Zeng, J. Miao, Y. Cao, X. Zhang, G. Tian and X. Bian, *Acta Biomater.*, 2022, **141**, 364–373.
91 C. Fang, Z. Deng, G. Cao, Q. Chu, Y. Wu, X. Li, X. Peng and G. Han, *Adv. Funct. Mater.*, 2020, **30**, 1910085.
92 J. Yu, Z. Wei, Q. Li, F. Wan, Z. Chao, X. Zhang, L. Lin, H. Meng and L. Tian, *Adv. Sci.*, 2021, **8**, 2101467.
93 Y. Zhao, R. Song, Z. Zhang, H. Hu, W. Ning, X. Duan, J. Jiao, X. Fu and G. Zhang, *Nanoscale Adv.*, 2024, **6**, 72–78.
94 G. Cheng, W. Li, L. Ha, X. Han, S. Hao, Y. Wan, Z. Wang, F. Dong, X. Zou, Y. Mao and S.-Y. Zheng, *J. Am. Chem. Soc.*, 2018, **140**, 7282–7291.

95 X. Lian, Y. Huang, Y. Zhu, Y. Fang, R. Zhao, E. Joseph, J. Li, J. Pellois and H. Zhou, *Angew. Chem., Int. Ed.*, 2018, **57**, 5725–5730.
96 X. Zhong, Y. Zhang, L. Tan, T. Zheng, Y. Hou, X. Hong, G. Du, X. Chen, Y. Zhang and X. Sun, *J. Controlled Release*, 2019, **300**, 81–92.
97 Q. Zuo, T. Li, L. Huang, Z. Liu and W. Xue, *Biomater. Sci.*, 2023, **11**, 5025–5045.
98 J. Guo, X. Du, J. Huang, C. Liu, Y. Zhou, Y. Li and B. Du, *Adv. Healthcare Mater.*, 2022, **11**, 2200859.
99 Z. Jiang, G. Cai, H. Liu, L. Liu, R. Huang, X. Nie, R. Gui, J. Li, J. Ma, K. Cao and Y. Luo, *J. Nanobiotechnol.*, 2024, **22**, 296.
100 L. Ding, X. Lin, Z. Lin, Y. Wu, X. Liu, J. Liu, M. Wu, X. Zhang and Y. Zeng, *ACS Appl. Mater. Interfaces*, 2020, **12**, 36906–36916.
101 T. Huang, W.-L. Pan, M.-S. Li, Y.-M. Zou, W. Meng, M.-M. Li, W.-H. Zhang, Z. Dai, J.-X. Chen and J. Chen, *ACS Mater. Lett.*, 2024, **6**, 498–507.
102 M. Chen, T. Xu, L. Song, T. Sun, Z. Xu, Y. Zhao, P. Du, L. Xiong, Z. Yang, J. Jing and H. Shi, *Theranostics*, 2024, **14**, 5461–5491.
103 Y.-Z. Jing, S.-J. Li and Z.-J. Sun, *J. Mater. Chem. B*, 2021, **9**, 8541–8557.
104 Y. Zhou, T. Yang, K. Liang and R. Chandrawati, *Adv. Drug Delivery Rev.*, 2021, **171**, 199–214.
105 Y. Wang, T. Yang and Q. He, *Natl. Sci. Rev.*, 2020, **7**, 1485–1512.
106 J. Zhang, X. Cao, H. Wen, Q. T. H. Shubhra, X. Hu, X. He and X. Cai, *Coord. Chem. Rev.*, 2025, **539**, 216746.
107 L. Guan, F. Liu, C. Zhang, W. Wang, J. Zhang and Q. Liang, *Adv. Sens. Energy Mater.*, 2024, **3**, 100123.
108 H. Zhang, X.-T. Tian, Y. Shang, Y.-H. Li and X.-B. Yin, *ACS Appl. Mater. Interfaces*, 2018, **10**, 28390–28398.
109 Y. Cao, M. Zheng, Q. Zhou, Y. Dong, Y. Hou and Z. Ge, *ACS Appl. Mater. Interfaces*, 2025, **17**, 44263–44274.
110 Z. Jin, P. Zhao, J. Zhang, T. Yang, G. Zhou, D. Zhang, T. Wang and Q. He, *Chem. – Eur. J.*, 2018, **24**, 11667–11674.
111 X. Cai, Z. Xie, B. Ding, S. Shao, S. Liang, M. Pang and J. Lin, *Adv. Sci.*, 2019, **6**, 1900848.
112 W. Zhou, J. Zhang, W. Chen and C. Miao, *J. Cancer Res. Clin. Oncol.*, 2024, **150**, 170.
113 G. Zhou, Y. S. Wang, Z. Jin, P. Zhao, H. Zhang, Y. Wen and Q. He, *Nanoscale Horiz.*, 2019, **4**, 1185–1193.
114 J. An, Y.-G. Hu, C. Li, X.-L. Hou, K. Cheng, B. Zhang, R.-Y. Zhang, D.-Y. Li, S.-J. Liu, B. Liu, D. Zhu and Y.-D. Zhao, *Biomaterials*, 2020, **230**, 119636.
115 S.-S. Wan, J.-Y. Zeng, H. Cheng and X.-Z. Zhang, *Biomaterials*, 2018, **185**, 51–62.
116 J. Yao, Y. Liu, J. Wang, Q. Jiang, D. She, H. Guo, N. Sun, Z. Pang, C. Deng, W. Yang and S. Shen, *Biomaterials*, 2019, **195**, 51–62.
117 Q. Dai, L. Wang, E. Ren, H. Chen, X. Gao, H. Cheng, Y. An, C. Chu and G. Liu, *Angew. Chem., Int. Ed.*, 2022, **61**, e202211674.
118 Y. Wang, D. Jing, J. Yang, S. Zhu, J. Shi, X. Qin, W. Yin, J. Wang, Y. Ding, T. Chen, B. Lu and Y. Yao, *Acta Biomater.*, 2022, **154**, 467–477.
119 Y. Yang, N. Wang, Z. Wang, M. Han, F. Yan, Z. Shi and S. Feng, *Chem. Eng. J.*, 2023, **474**, 145764.
120 X. Chen, Q. Tang, J. Wang, Y. Zhou, F. Li, Y. Xie, X. Wang, L. Du, J. Li, J. Pu, Q. Hu, Z. Gu and P. Liu, *Adv. Mater.*, 2023, **35**, 2210440.
121 M. Liu, C. Sun, J. Jiang, L. Wan, C. Hu, C. Wen, G. Huang, Q. Ruan, S. Wu, D. Qiao, P. Zheng, Q. Pan and W. Zhu, *ACS Appl. Nano Mater.*, 2023, **6**, 21587–21602.
122 W. Liu, C. Sun, Y. Dai, H. Wang, M. Ashrafizadeh, J. Conde, L. Yang and W. He, *Mater. Today Bio*, 2025, **34**, 102183.
123 X. Zhao, H. Cheng, Q. Wang, W. Nie, Y. Yang, X. Yang, K. Zhang, J. Shi and J. Liu, *ACS Nano*, 2023, **17**, 13746–13759.
124 Z. Cai, F. Xin, Z. Wei, M. Wu, X. Lin, X. Du, G. Chen, D. Zhang, Z. Zhang, X. Liu and C. Yao, *Adv. Healthcare Mater.*, 2020, **9**, 1900996.
125 L. Dai, M. Yao, Z. Fu, X. Li, X. Zheng, S. Meng, Z. Yuan, K. Cai, H. Yang and Y. Zhao, *Nat. Commun.*, 2022, **13**, 2688.
126 C. Yang, H. Ming, B. Li, S. Liu, L. Chen, T. Zhang, Y. Gao, T. He, C. Huang and Z. Du, *J. Controlled Release*, 2024, **376**, 659–677.
127 P. Wang, M. Xiao, H. Pei, H. Xing, S.-H. Luo, C.-K. Tsung and L. Li, *Chem. Eng. J.*, 2021, **415**, 129036.
128 X. Lin, H. Wu, J. Zhang, X. Chen, X. Gao and Y. Liu, *Chem. Eng. J.*, 2024, **480**, 147865.
129 H. Wang, S. Li, L. Wang, Z. Liao, H. Zhang, T. Wei and Z. Dai, *Chem. Eng. J.*, 2023, **456**, 140963.
130 Y. Sun, Z. Ren, Z. Zhang, K. Yang, Y. Jin, H. Deng, Y. Liu, J. Wang, P. Ji and P. Liu, *Sci. Rep.*, 2025, **15**, 9791.
131 N. Tyagi, Y. H. Wijesundara, J. J. Gassensmith and A. Popat, *Nat. Rev. Mater.*, 2023, **8**, 701–703.
132 A. Schuhmacher, M. Hinder, E. Brief, O. Gassmann and D. Hartl, *Drug Discovery Today*, 2025, **30**, 104291.
133 A. Wang, M. Walden, R. Ettlinger, F. Kiessling, J. J. Gassensmith, T. Lammers, S. Wuttke and Q. Peña, *Adv. Funct. Mater.*, 2024, **34**, 2308589.